SESAME SUNSTONE Training Programme - First Edition

Apr 29, 2025

Operando XAFS measurements at the BM08-XAFS/XRF beamline

Messaoud Harfouche

BM08-XAFS/XRF Beamline Senior Scientist

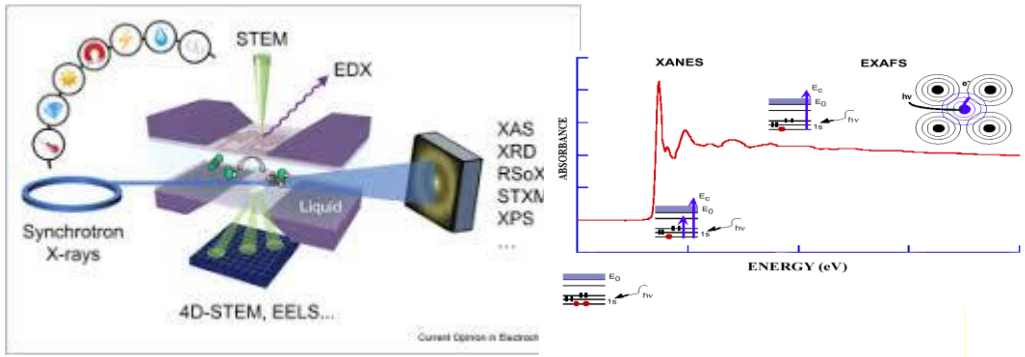

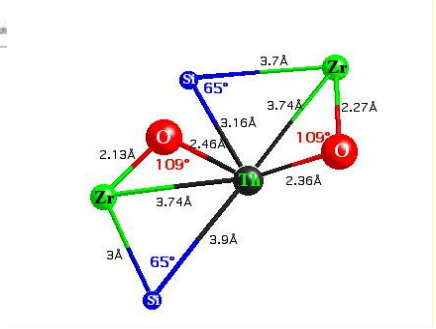

SESAME SUNSTONE Training Programme - First Edition

Apr 29, 2025

In-Situ XAFS measurements at the BM08-XAFS/XRF beamline

Messaoud Harfouche

BM08-XAFS/XRF Beamline Senior Scientist

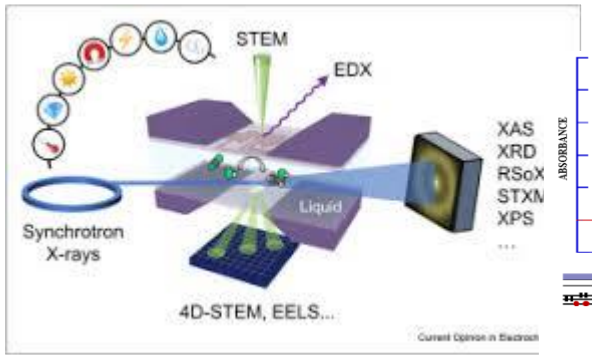

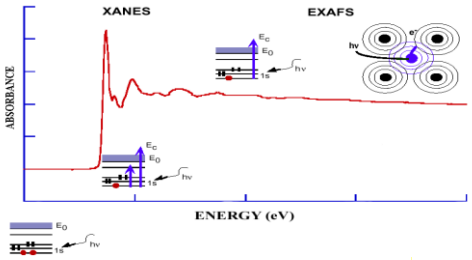

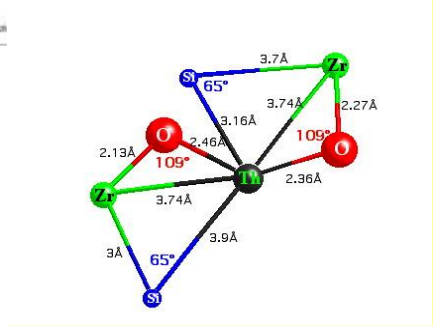

Synchrotron light sources around the World

Synchrotron radiation sources properties

Broad Spectrum which covers from microwaves to hard X-rays: the user can select the wavelength required for experiment;

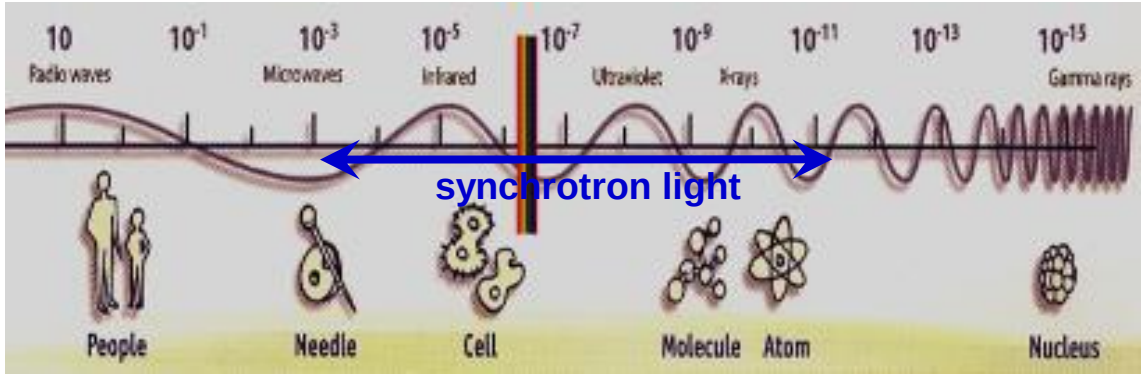

High Flux: high intensity photon beam, allows rapid experiments or use of weakly scattering crystals;

$$\text{Flux} = \text{Photons} / (s \bullet \text{BW})$$

High Brilliance (Spectral Brightness): highly collimated photon beam generated by a small divergence and small size source (partial coherence);

$$\text{Brilliance} = \text{Photons} / (s \bullet mm^2 \bullet mrad^2 \bullet \text{BW})$$

High Stability: submicron source stability

Tunability: easy change of the wavelength (energy)

Polarisation: both linear and circular (with IDs)

Pulsed Time Structure: pulsed length down to tens of picoseconds allows the resolution of process on the same time scale

Synchrotron Radiation Facility

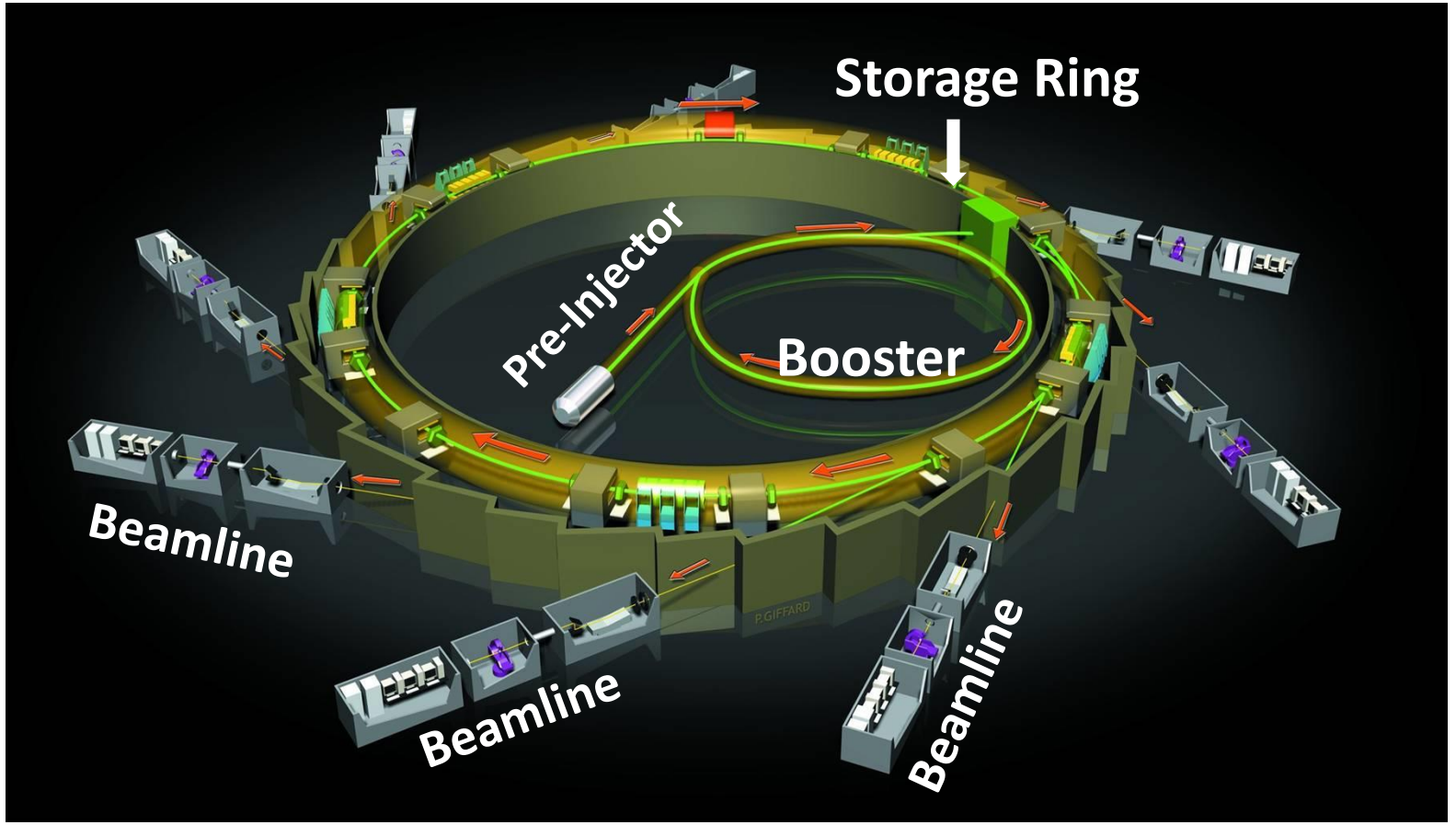

layout of atypical synchrotron

All beamlines get beam simultaneously

Brief History of SESAME

- 1980's: Noble Loreate **Adbus Salam** suggested a light source for the Middle East
- 1990's: Individuals and groups promote scientific cooperation between countries with conflicts in the Middle East
  - Middle East Scientific Cooperation (MESC) group, Sergio Fubini, Herwik Schopper, …
- 1997: **Gus Voss and Herman Wenick** proposed to re-use BessyI accelerator for the Middle East.

Brief History of SESAME

- **2008:** Installation of the **Microtron**
- **2009: first beam** from the Microtron (low energy beam ~9 MeV) … *Temporally shielding*
- **2011: Full beam** from the Microtron (22 MeV) … … *after completion of the wall shielding*
- **2014:** Start commissioning the **Booster**
- **2016:** Commissioning of the 2.5 GeV storage ring
- **2017:**
  - ✓ First beam in the **storage ring**
  - ✓ First **monochromatic** light in the XAFS/XRF beamline and first EXAFS spectrum
  - ✓ Inauguration (**opening ceremony**)
- **2018:** First SR-IR and first IR spectrum

SESAME Machine

Shielding wall and roof

3D drawing of the SESAME Building

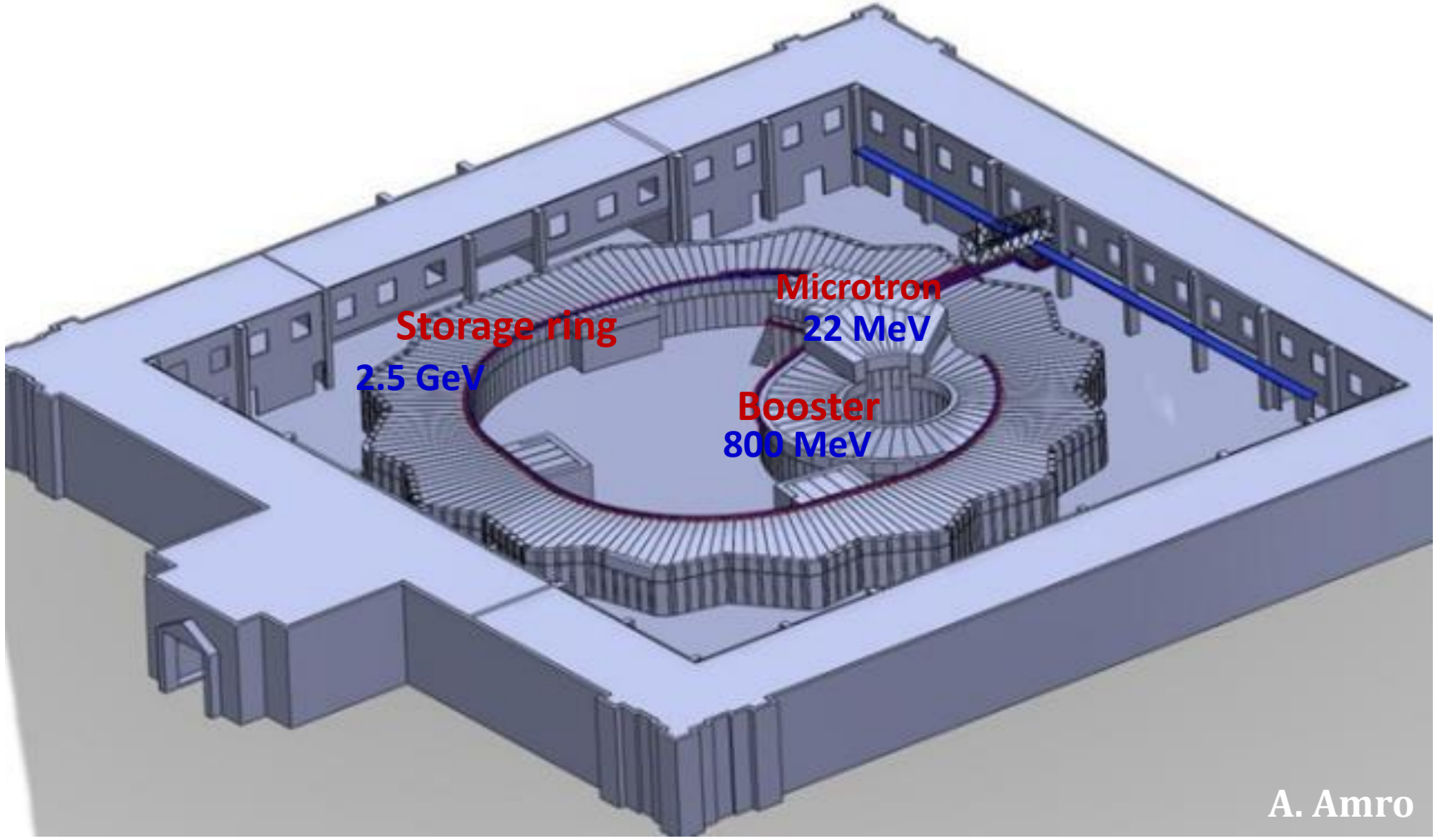

Machine Parameters

Parameter	Unit	Value
Energy	GeV	2.5
Circumference	m	133.2
Current	mA	400
Beam Liftime	hr	21.5
Magnetic field (BM)	T	1.45
Critical energy	eV	6049.4

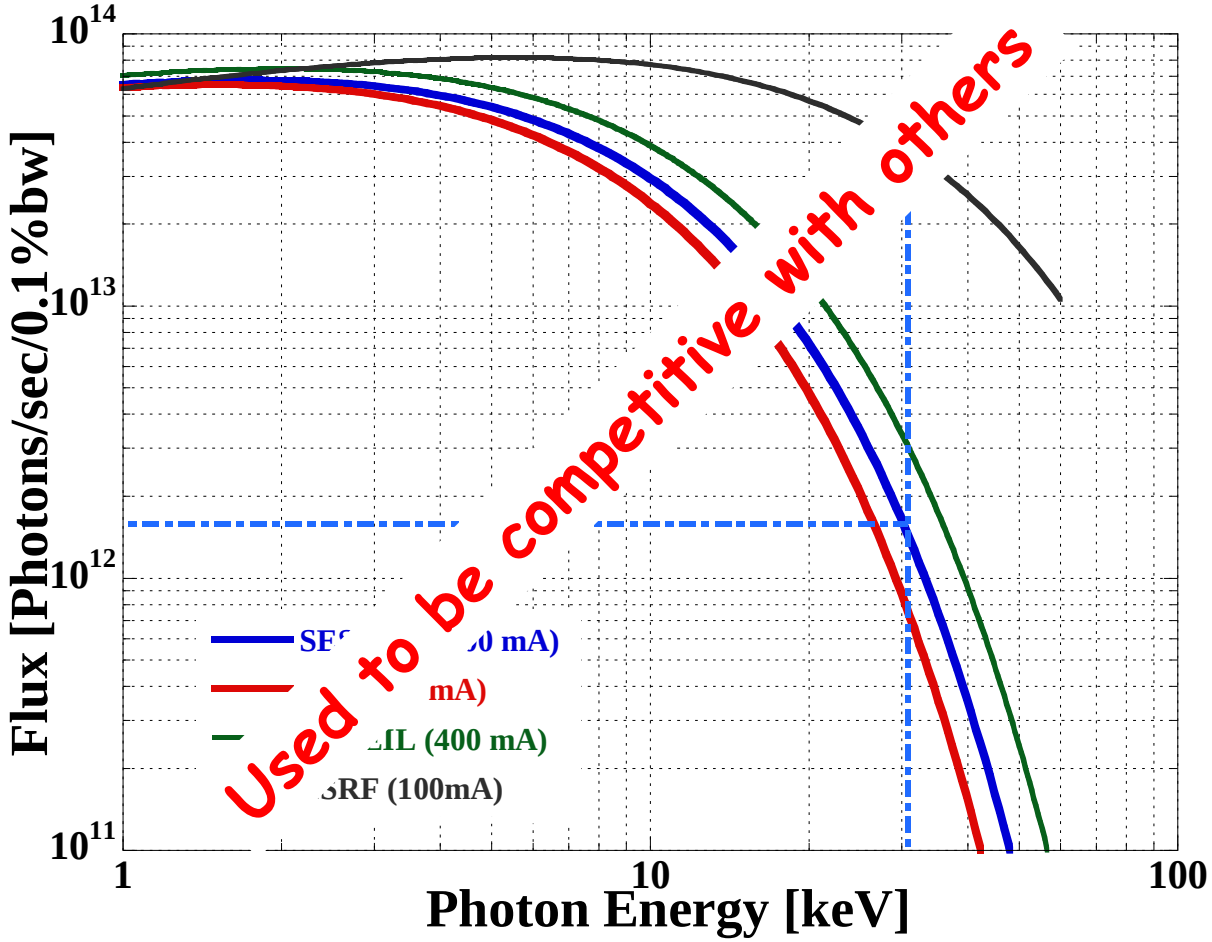

SESAME machine was comparable to world class machines
SOLEIL, France and **SLS** Switzerland

BM08-XAFS/XRF Beamline

Beamline Scientists: **Messaoud Harfouche**
Latif Ullah Khan

Status: Operational since November 2017

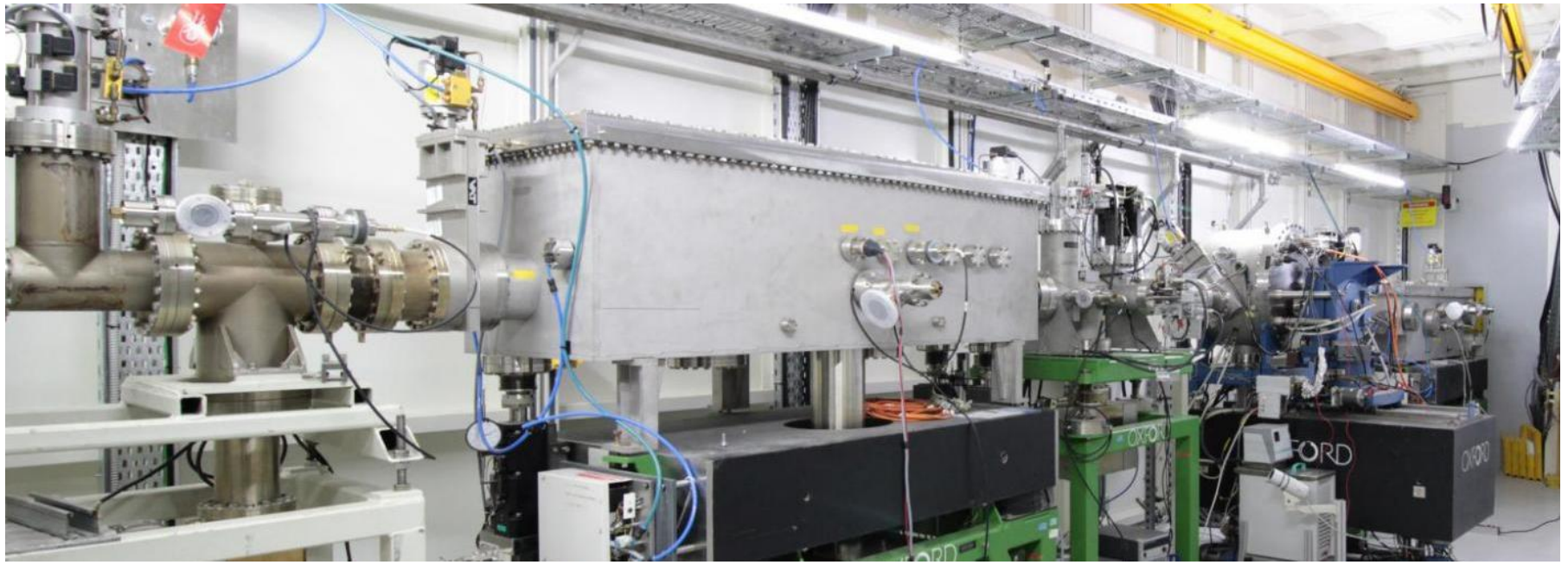

Most of the optics components are donations (ROBL)

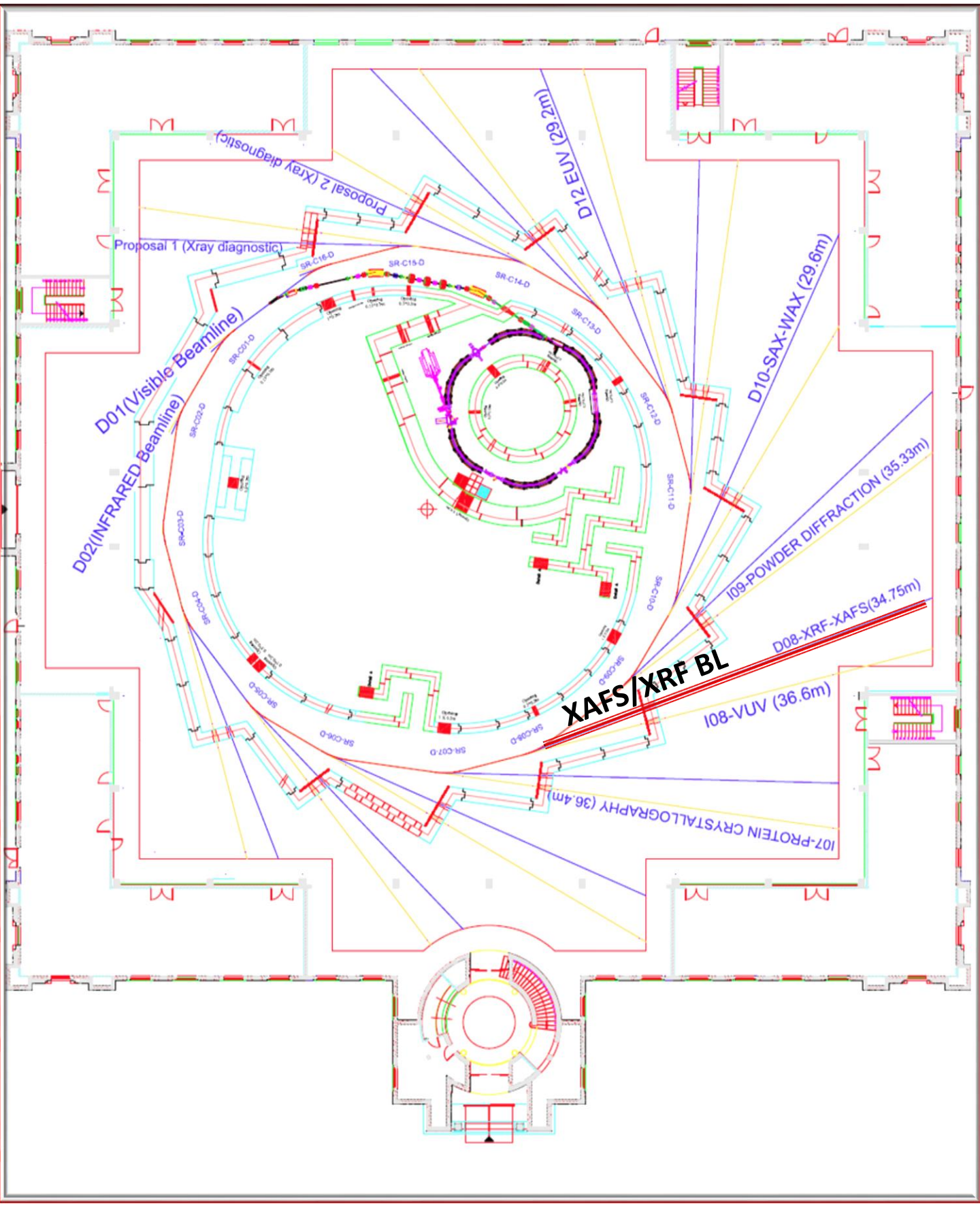
Proposal 2 (Xray diagnostic)
Proposal 1 (Xray diagnostic)
D12 EUV (29.2m)
D10-SAX-WAX (29.6m)
I09-POWDER DIFFRACTION (35.33m)
D08-XRF-XAFS(34.75m)
I08-VUV (36.6m)
I07-PROTEIN CRYSTALLOGRAPHY (36.4m)
D01(Visible Beamline)
D02(INFRARED Beamline)
XAFS/XRF BL
SR-C16-D
SR-C15-D
SR-C14-D
SR-C13-D
SR-C12-D
SR-C11-D
SR-C10-D
SR-C09-D
SR-C08-D
SR-C07-D
SR-C06-D
SR-C05-D
SR-C04-D
SR-C03-D
SR-C02-D
SR-C01-D

Brief History of the XAFS/XRF beamline

Task	Period
Conceptual Design Report	**July 2012**
Technical Design Report	**October 2014**
Installation (Pb Hutches, Optics)	**March 2016**
Control and alignment	**2015-July 2017**
Call for proposals (Sem-0)	**March, 2017 (36 submitted, 19 accepted)**
FE installation	**April-September 2017**
Start BL commissioning	**October 2017**
First Monochromatic beam	**November 2017**
First Scan	**November 2017**
End BL commissioning	**July 2018 (*only 3 months of operation*)**
First non-official User	**April 2018**
Official beamtime for Users	**July 2018**
Second call for proposals (Sem-1)	**October 2018 (61 submitted, 36 accepted)**

XAFS/XRF beamline optics

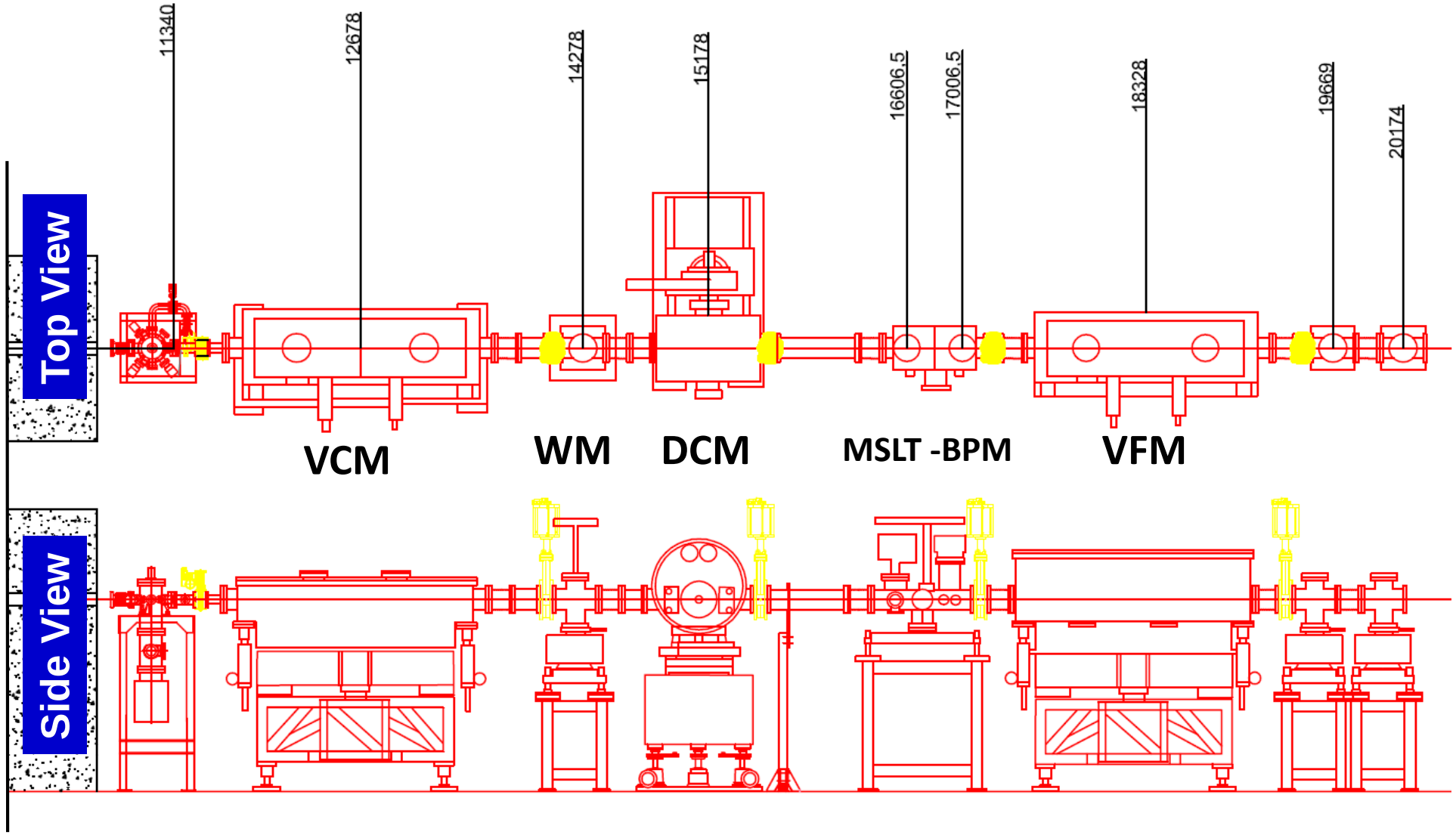

BM08-XAFS/XRF Beamline at SESAME

(operational since 2018)

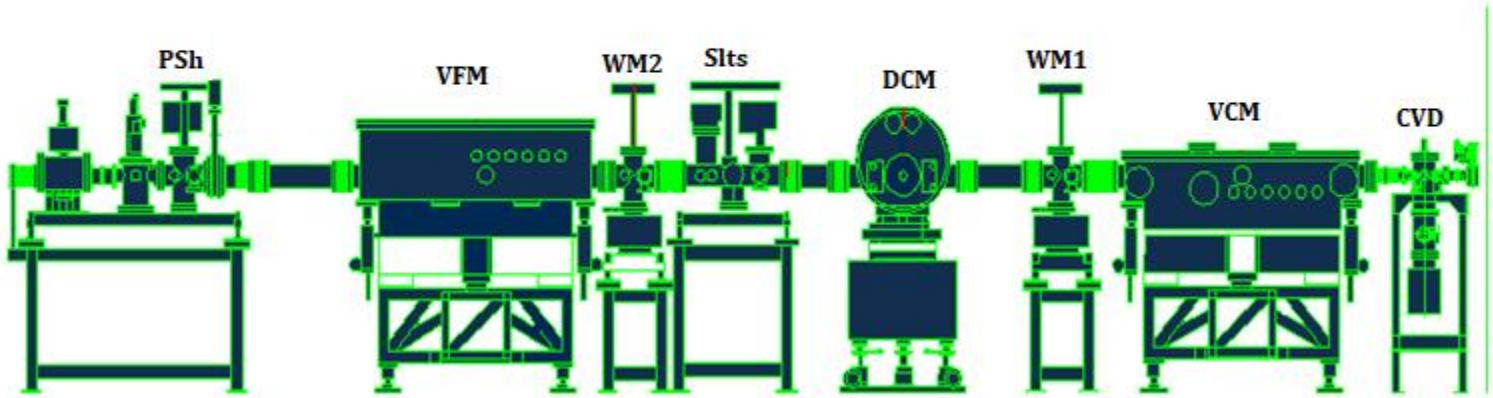

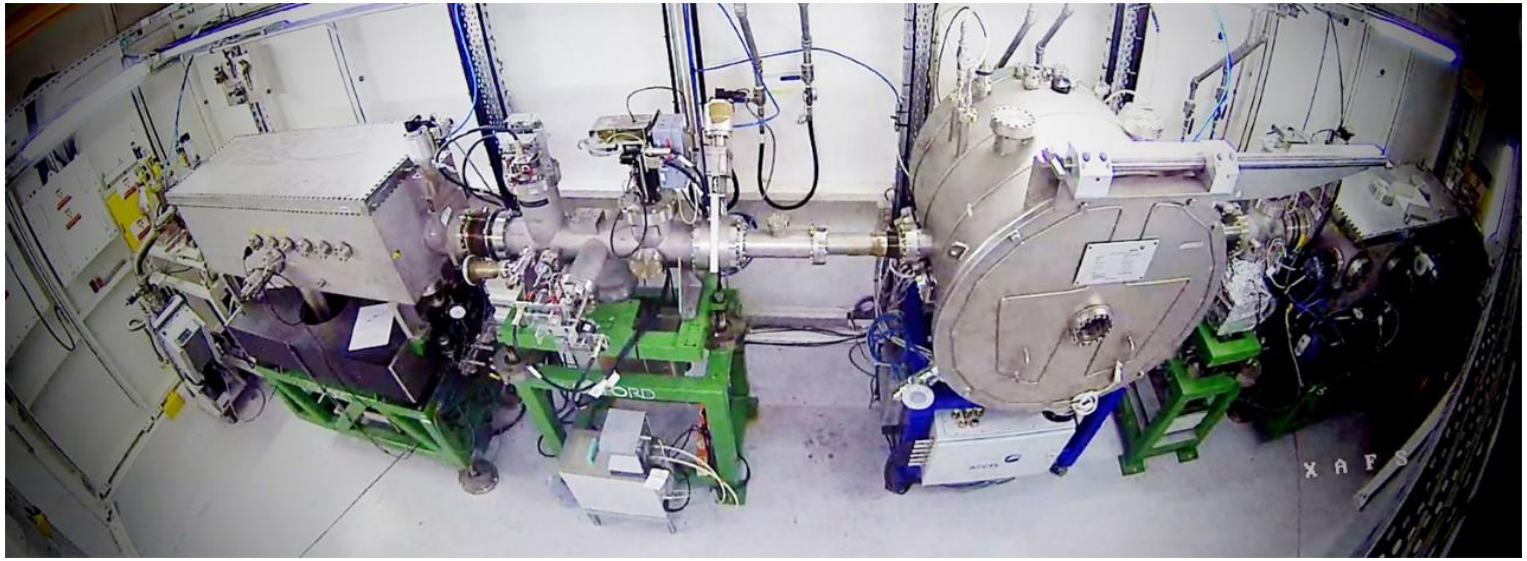

Design Parameters

Parameter	Unit	Value
Source (BM)	T	1.45
Hor. acceptance	mrad	3
Vert. acceptance	mrad	0.6
Energy range	keV	4.7 – 30
Energy resolution	-	~ 10^{-4}
Photon flux (S1)	Ph/sec	2x10^{12} (8keV)
~~Beam size (S1)~~	~~mm^2~~	~~~0.1 x 0.1~~
~~Beam size (S2)~~	~~μm^2~~	~~8x10~~
~~Photon flux (S2)~~	~~Ph/sec~~	~~5x10^9 (8keV)~~

No focusing system ➔ Use slits

2x2 mm^2 to 5 x 20 mm^2

BM08-XAFS/XRF beamline optics

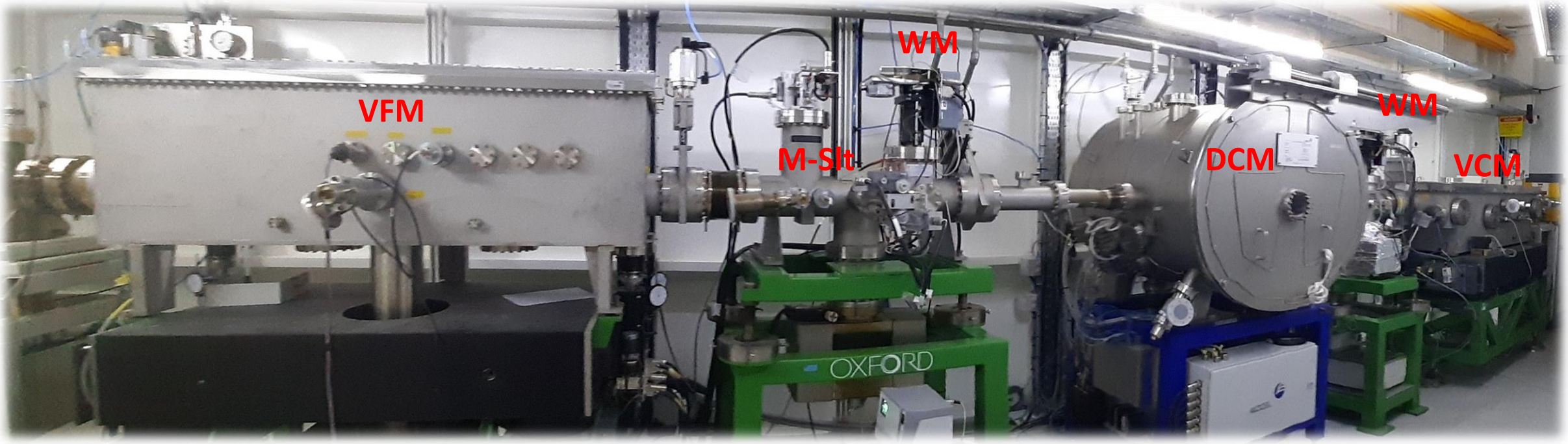

VCM: Vertical Collimating Mirror
DCM: Double crystal Monochromator
VFM : Vertical Focusing Mirror

WM: Wire Monitor
M-Slt: Monochromatic Slits

BM08-XAFS/XRF Beamline (EH)

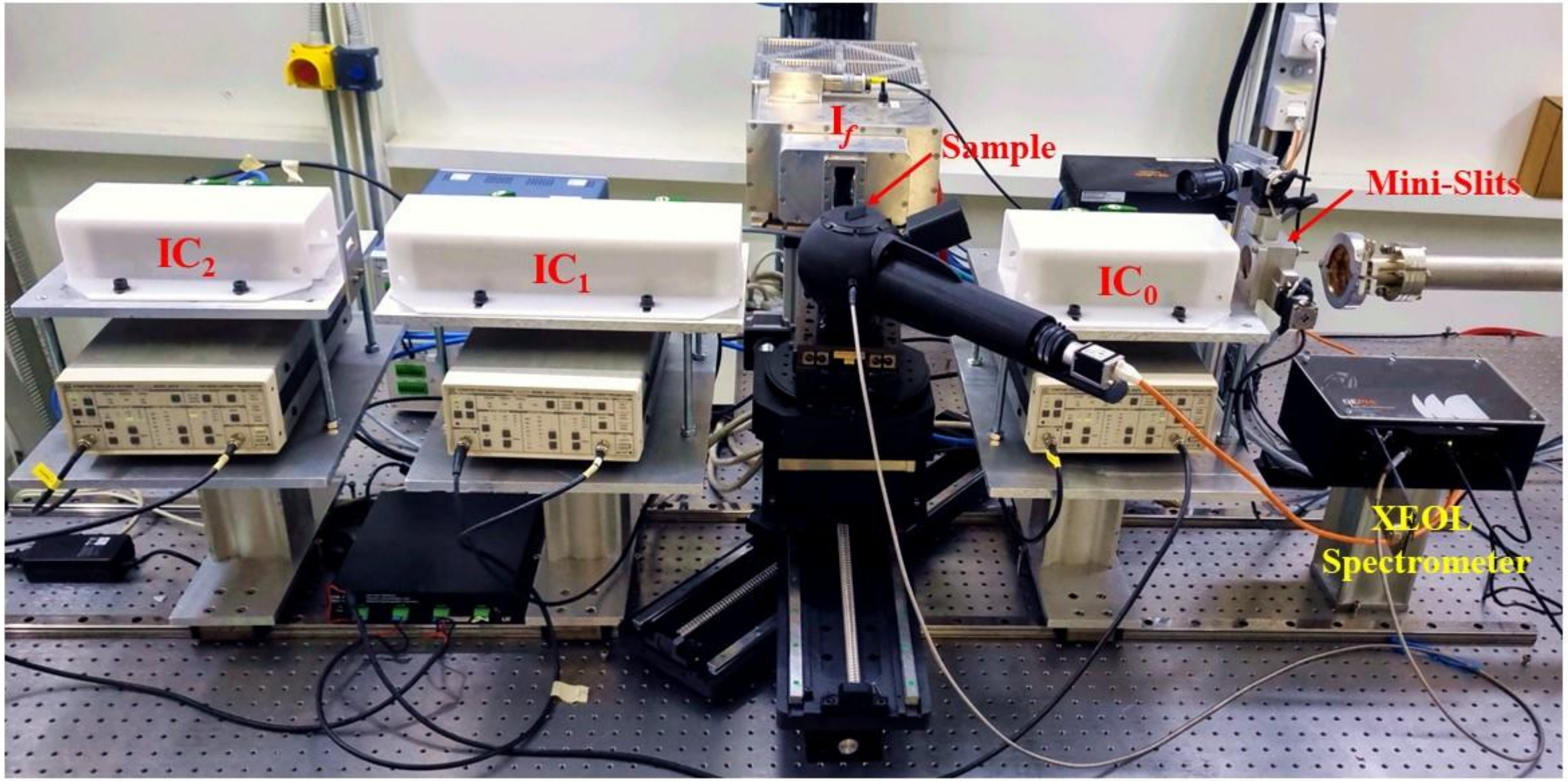

Experimental Station

6 Axis Motorized Positioning Stage
(Optics Focus)

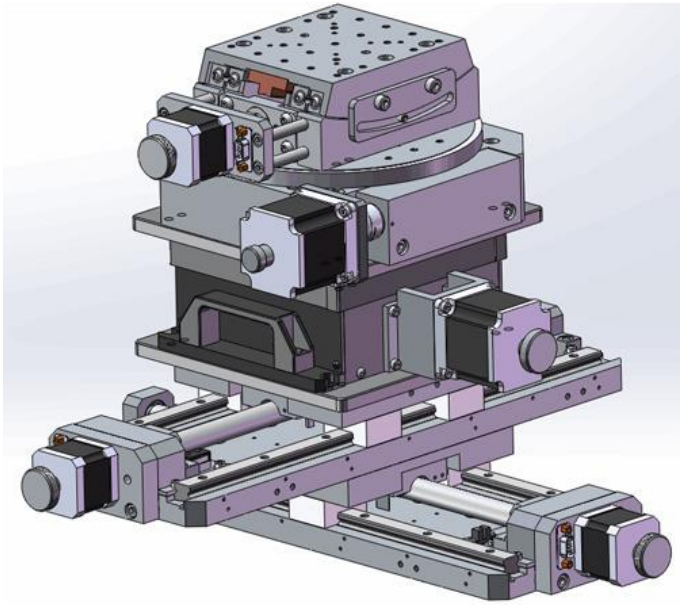

2 short ionization chambers
1 long IC for the I_{t2} (OKEN, Japan)

Experimental Station

A typical energy selective fluorescence spectrum:

Signal output	Low noise preamplifier **(XIA DXP)**
Output connector (analog)	LEMO FFS.00.250
Vacuum tightness	Optional; He leakage rate $<10^{-6}$ mbar · l/s
Number of channels	max. 8192
Peaking time range	0.1 to 24 µs in 24 steps
Software parameters	Digital gain, threshold, peaking time etc.
Signal form	Ramped reset type +1 V to -2 V; 5 mV/keV
Digital interfaces	USB 2.0, RS232 (on request)
Channel depth	24 bit
ADC	14 bit
Maximum read-out speed	1 ms (@1024 channels)
Clock frequency	40 MHz

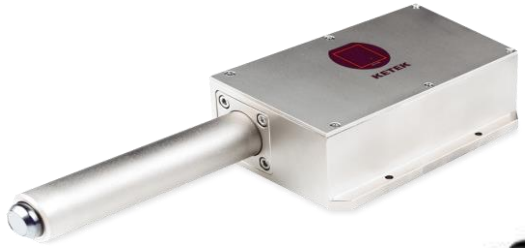

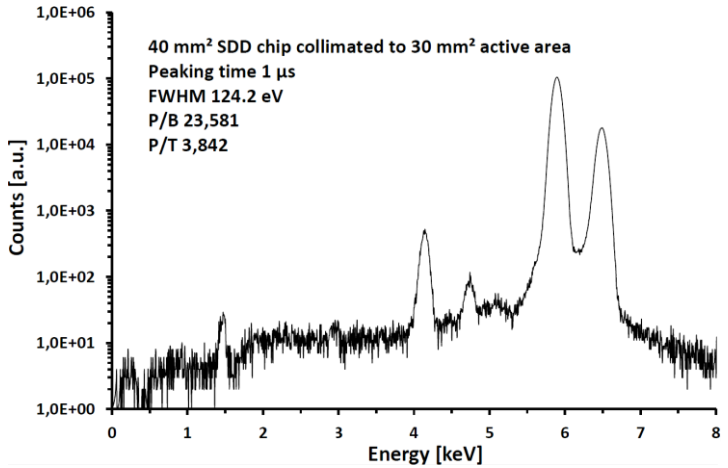

Fluorescence Detector : *64 Silicon Drift Detectors*

INFN Istituto Nazionale di Fisica Nucleare

Elettra Sincrotrone Trieste

INFN (Italy), Elettra (Italy) & SESAME

SESAME

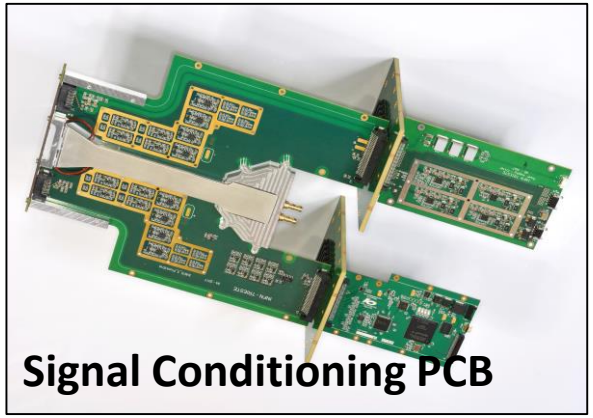

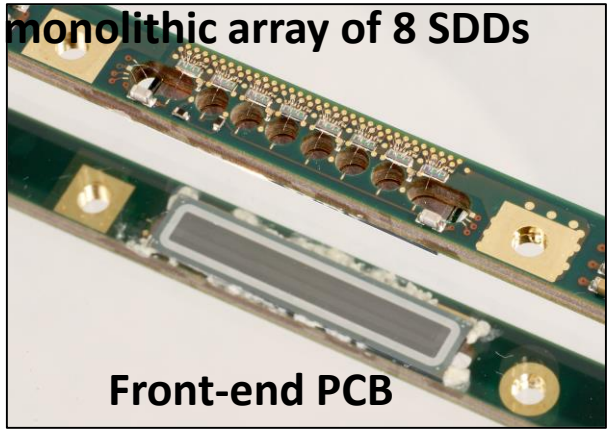

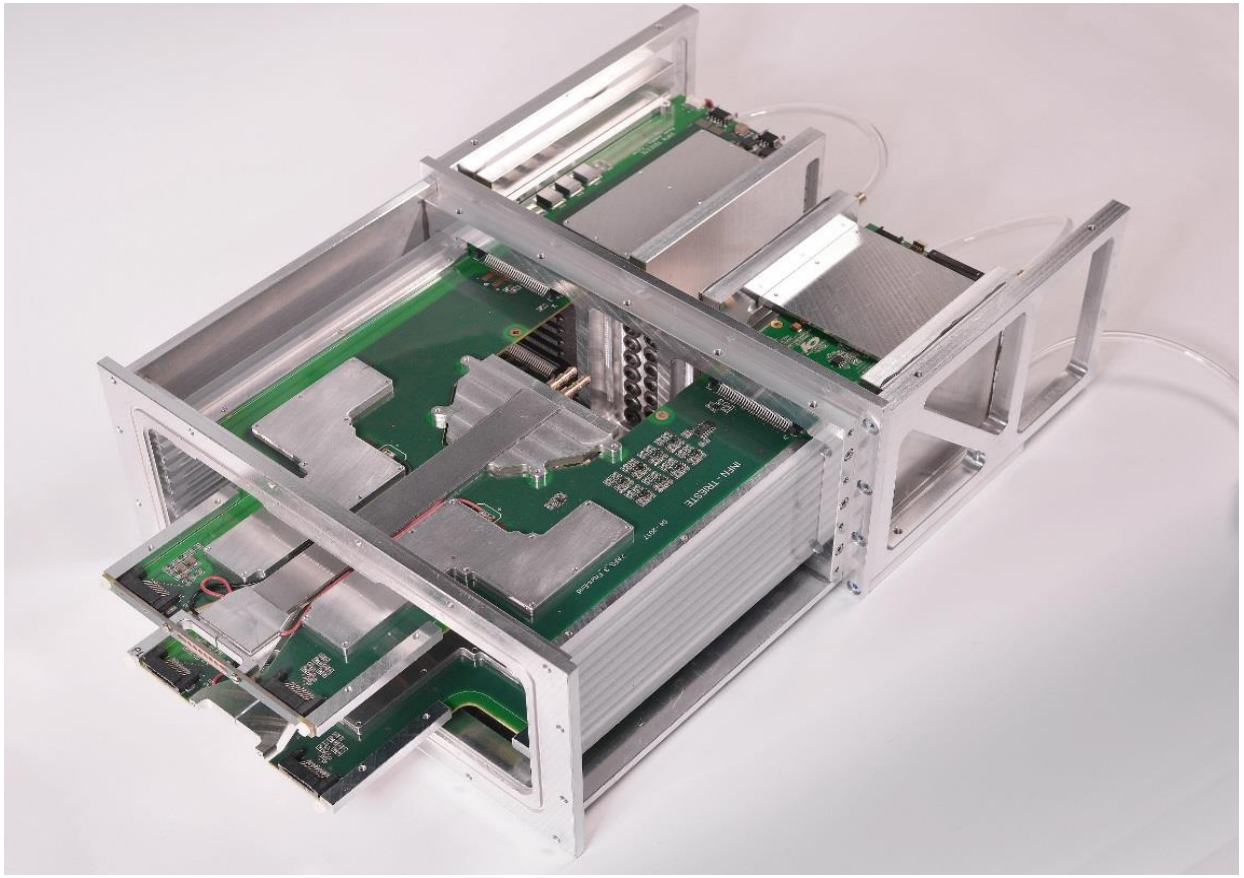

1. Front-end PCBs
2. Conditioning PCBs
3. Brass profile with cooling liquid flowing inside
4. Insertion guides at flanks of detecting heads
5. Rails for eight detection heads
6. Power supply and filters
7. Back-end PCBs
8. Inlet cooling distribution
9. Outlet cooling distribution
10. Ethernet PCBs
11. Power supply connectors

8 Modules x **8** SDDs with a Total collimated sensitive area of 499 mm^2

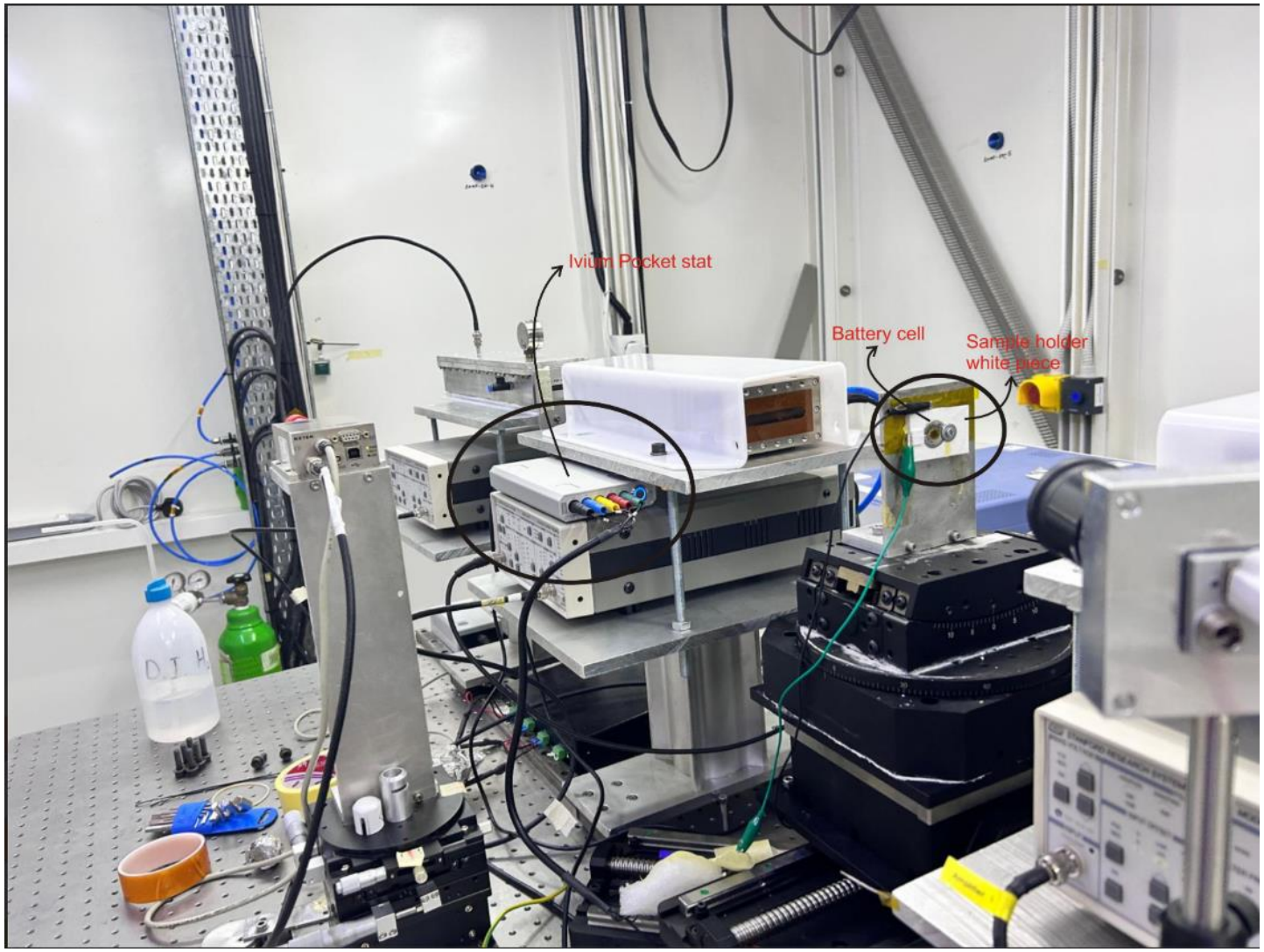
Ivium Pocket stat
Battery cell
Sample holder
white piece

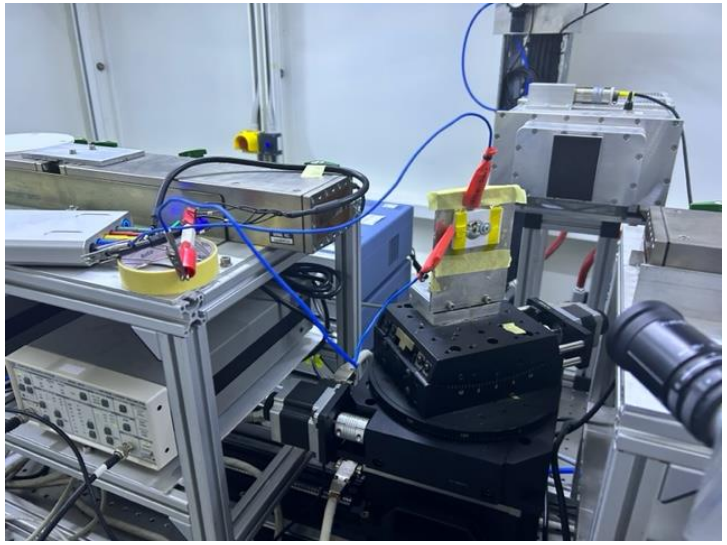

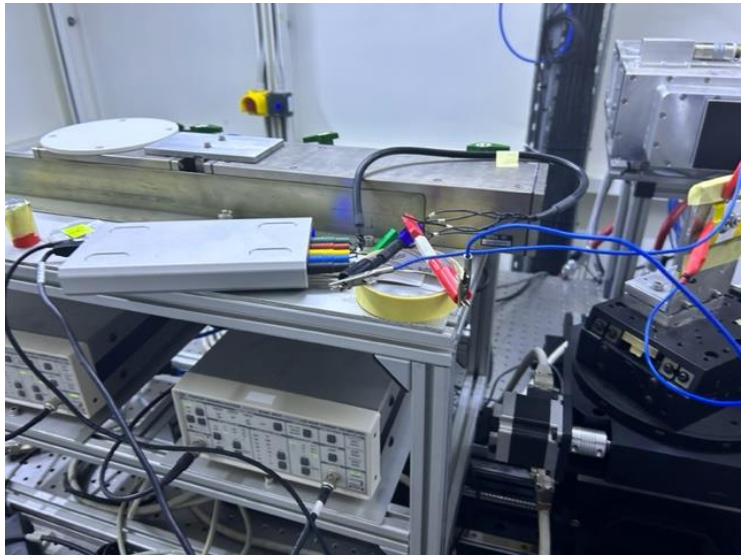

Sample Environment (*Shared between BLs*)

Air blower

800 °C

Cooling system (Cryojet)

95 Kelvin

Sample holders can be customized for special samples at SESAME's Mechanical Workshop

Sample Environment - Tubular Furnace/Reactor

- Tubular Furnace/Reactor: A Sample Environment for In-Operando X-ray Absorption Studies (Catalysis)

Temperature (ºC)	Sample Holder Ø mm	Atmospheres	Controller
Up to 800	8	Gases, Vapors and Vacuum	Programmable Logic Controller (PLC), SEASME

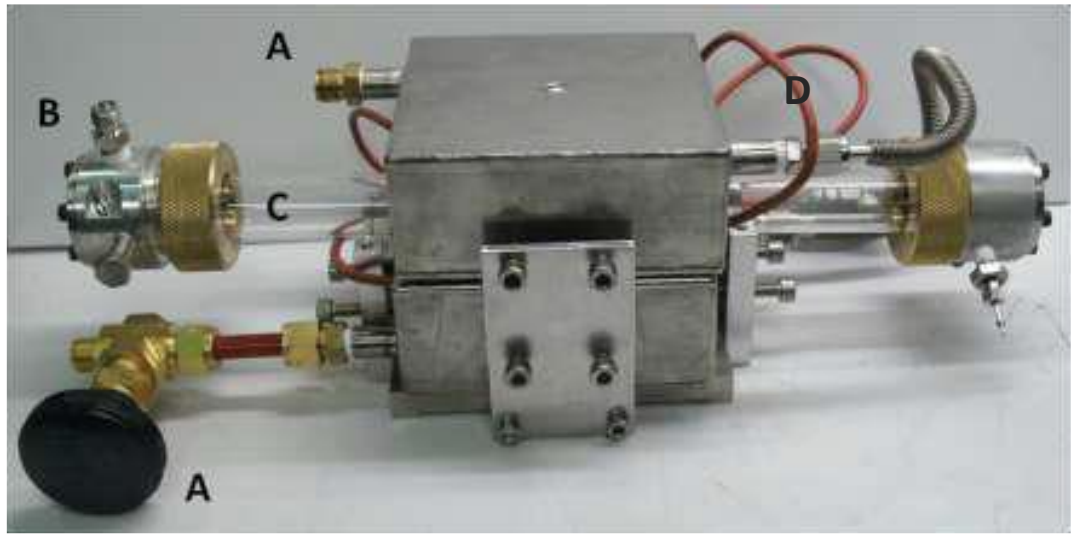

A: Inlet and outlet for water cooling
B: Inlet and outlet for gases with Kapton windows
C: Quartz glass tube

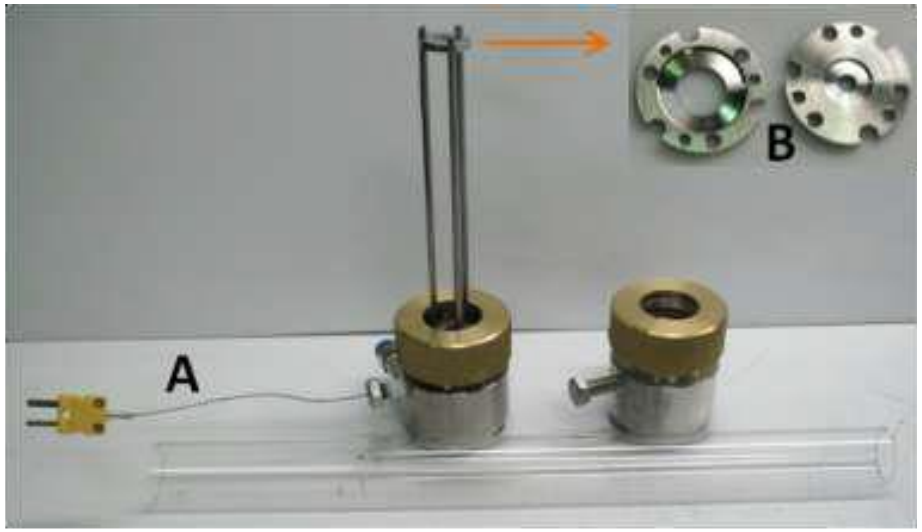

A: Thermocouple on the sample
B: End sample holder

Collaboration: Dr. Santiago J. A. Figueroa QUATI Beamline

Brazilian Synchrotron Light Laboratory

R-Fast scanning mode

Relatively

PandABox

OtF: 10 min

stp: 20 min

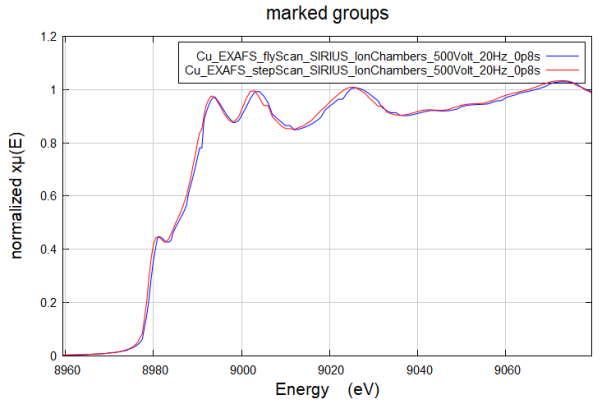

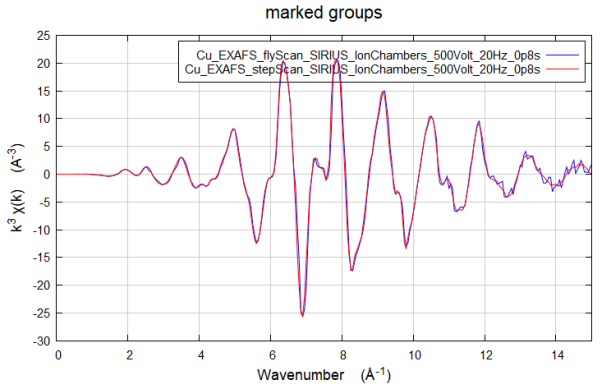

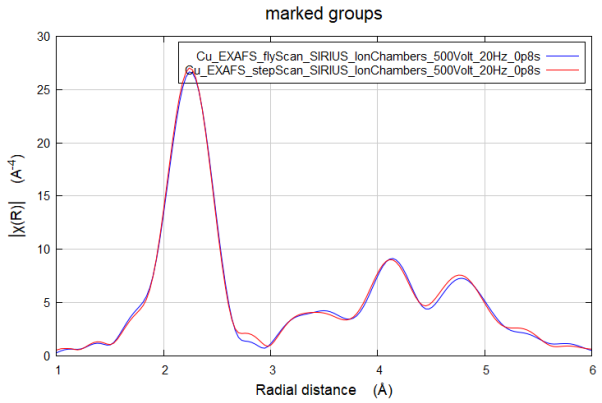

Almost NO difference between stp and OtF

Still Under Development

Prospective: X-ray Excited Optical Luminescence (XEOL)

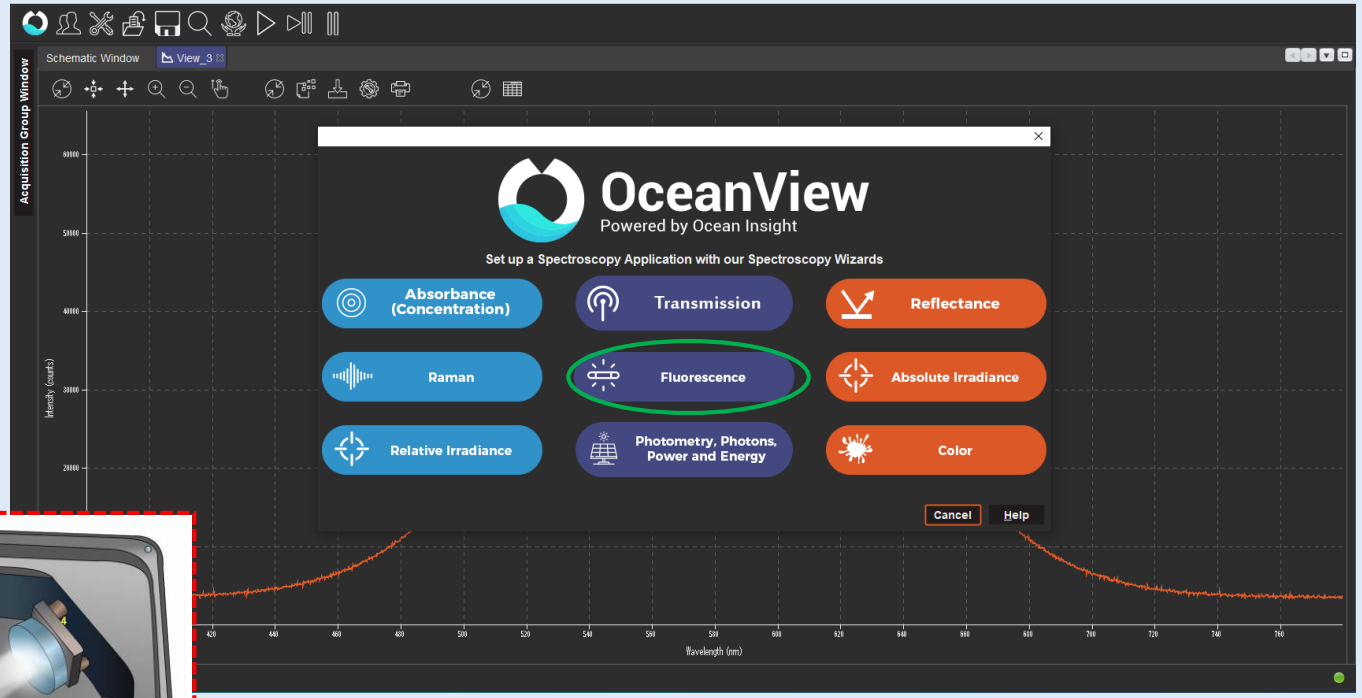

XEOL Setup

Collaboration between Jordan Atomic Energy Commission (JAEC) and XAFS/XRF Beamline

- **X-ray Excited Optical Luminescence (XEOL)** (λ: 200 - 920 nm)

Project Grant from IAEA

IAEA International Atomic Energy Agency

X-ray Excited Optical Luminescence (XEOL)

XEOL Spectrum

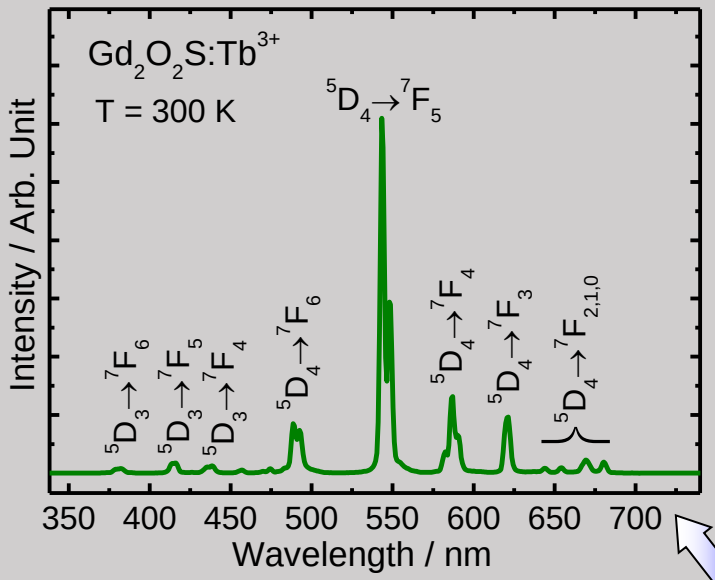

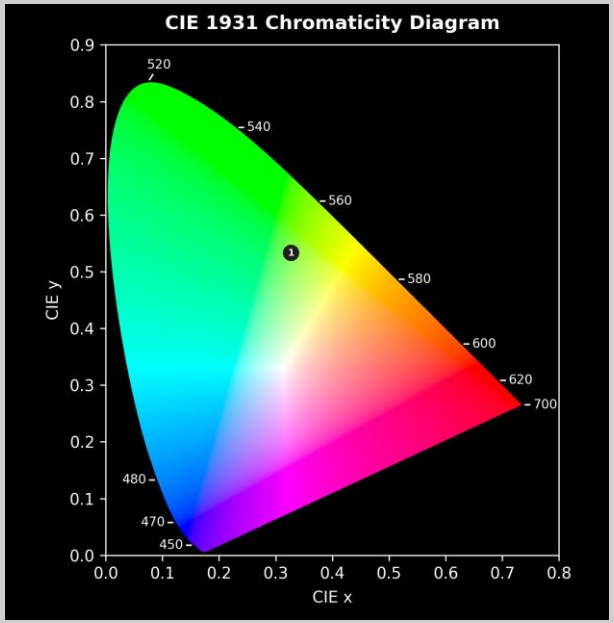

XEOL Spectrometer

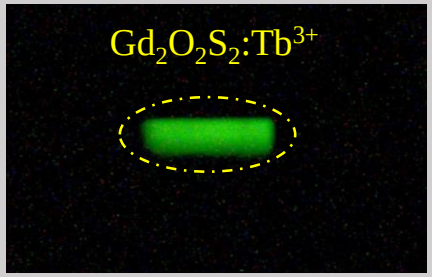

XEOL Sample Environment

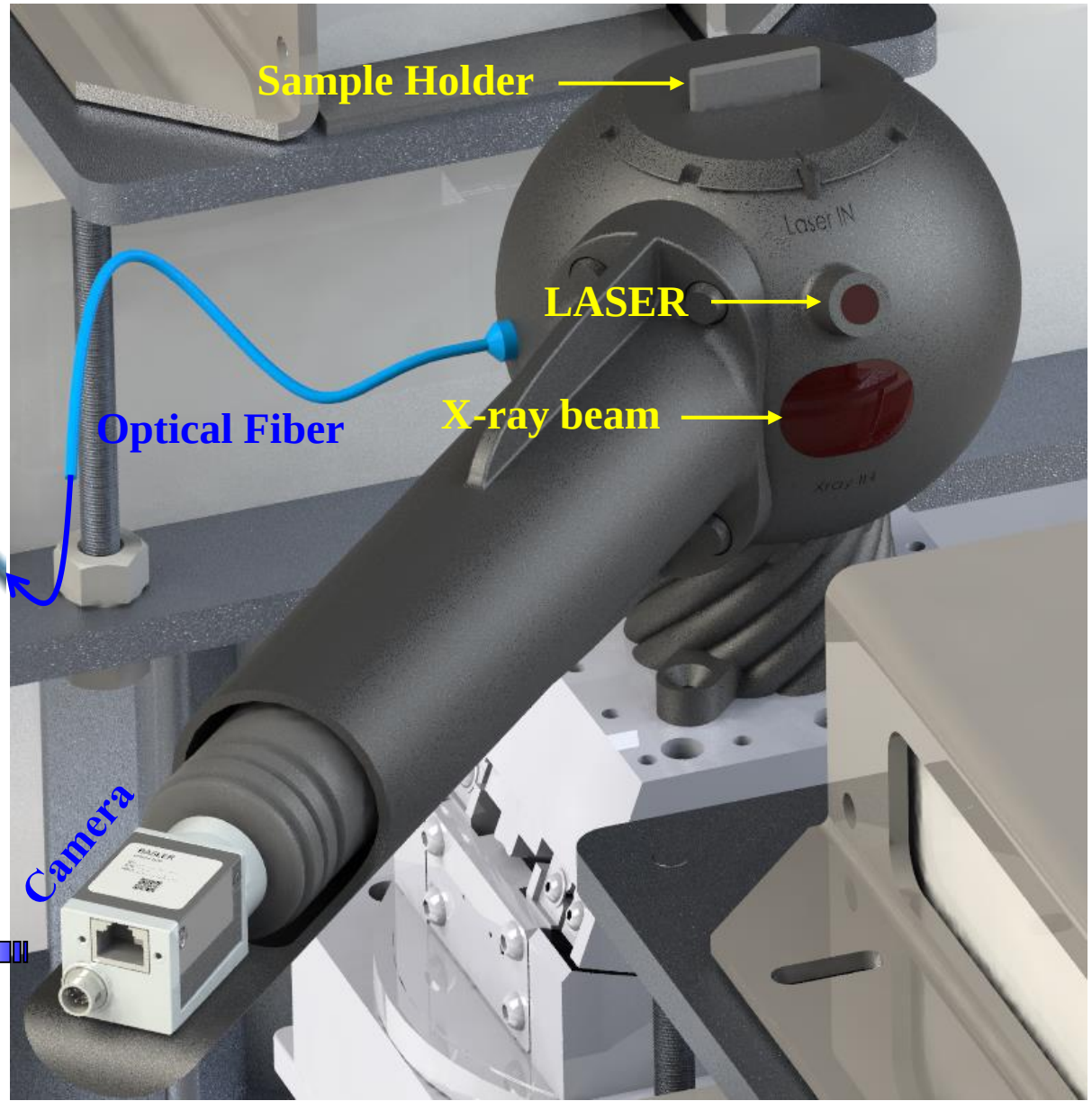

XAFS/XRF beamline: "Current Situation"

Si(111) & Si (311) Crystals

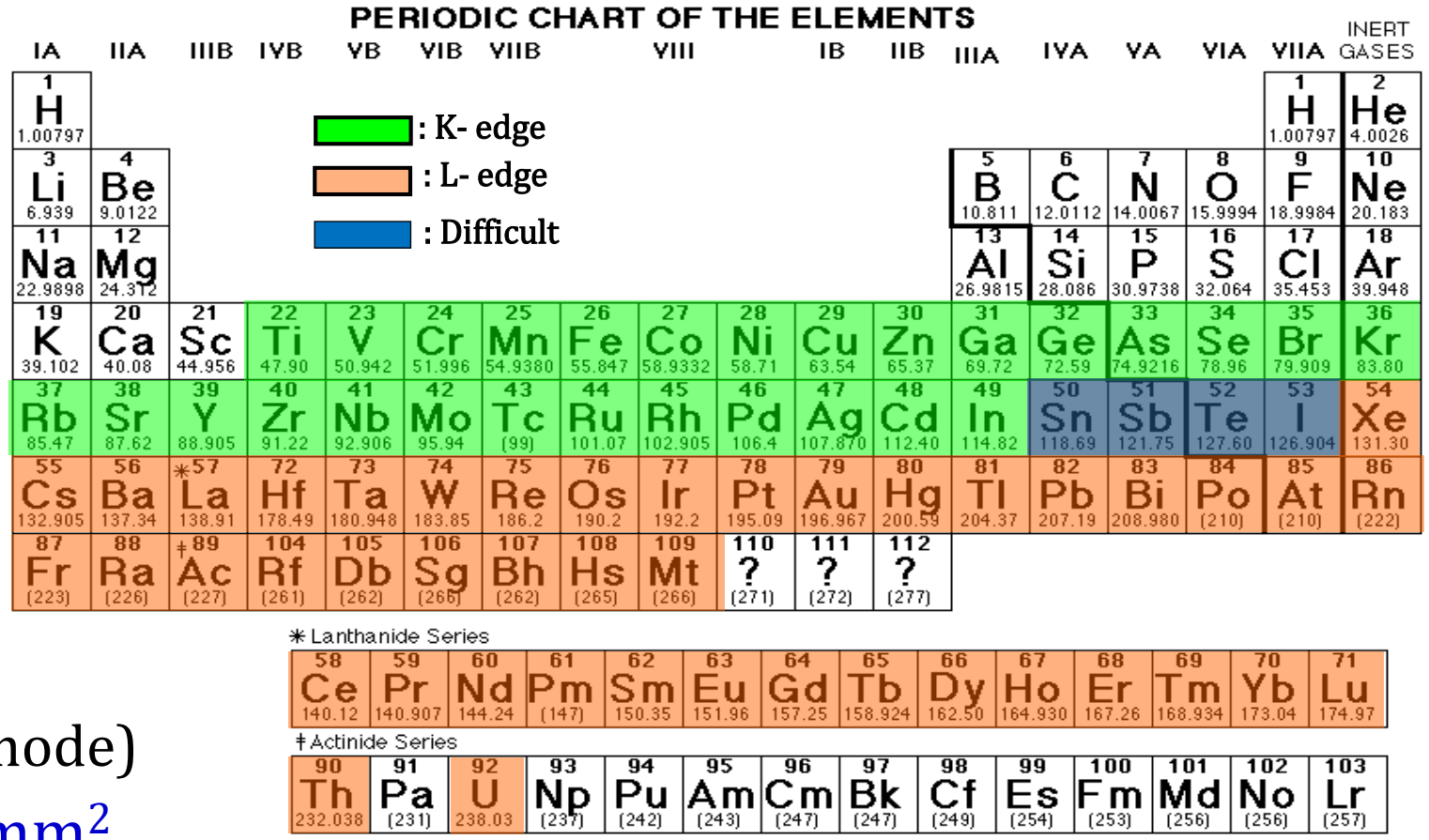

Beamline Characteristics

Energy range 4.7 – ~30 keV

Beam current 250 mA (decay mode)

Beam Size 2x2 mm^2 to 5 x 20 mm^2

Experimental Modes

- **Transmission mode**

$$\mu(E) = \log (I_0 / I_1)$$

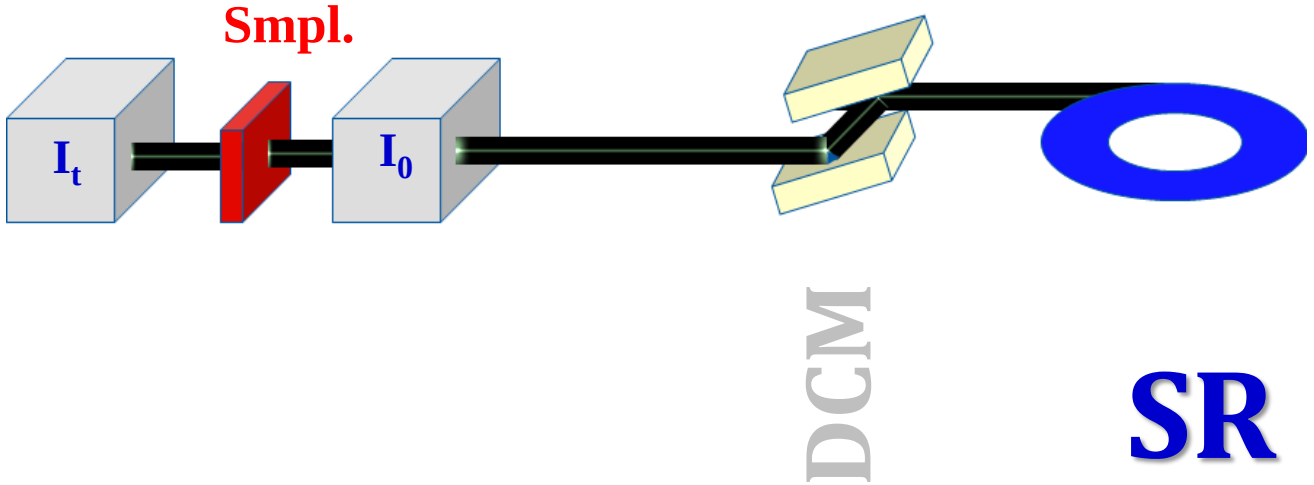

- **Fluorescence mode**

$$\mu(E) \sim I_f / I_0$$

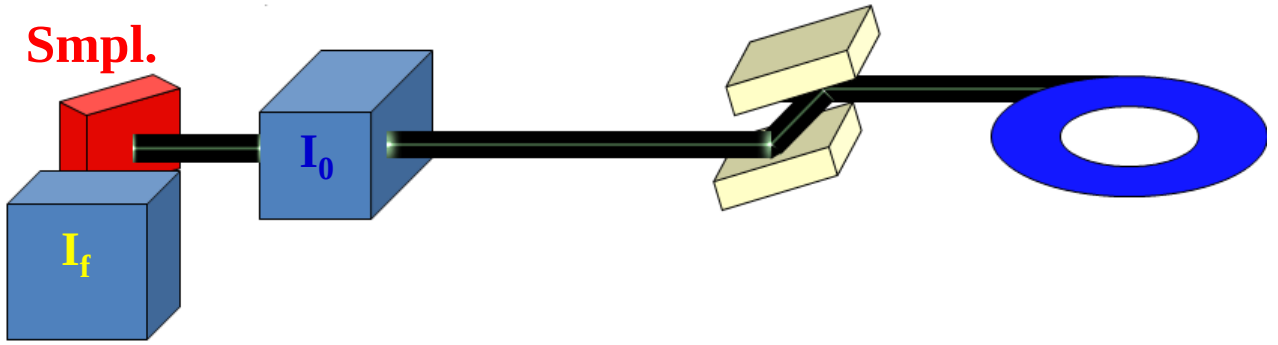

Re-filling of the deep core, generating a fluorescence, proportional to absorption

FUNDAMENTALS OF XRF & XAFS TECHNIQUES: XAFS PRINCIPLE

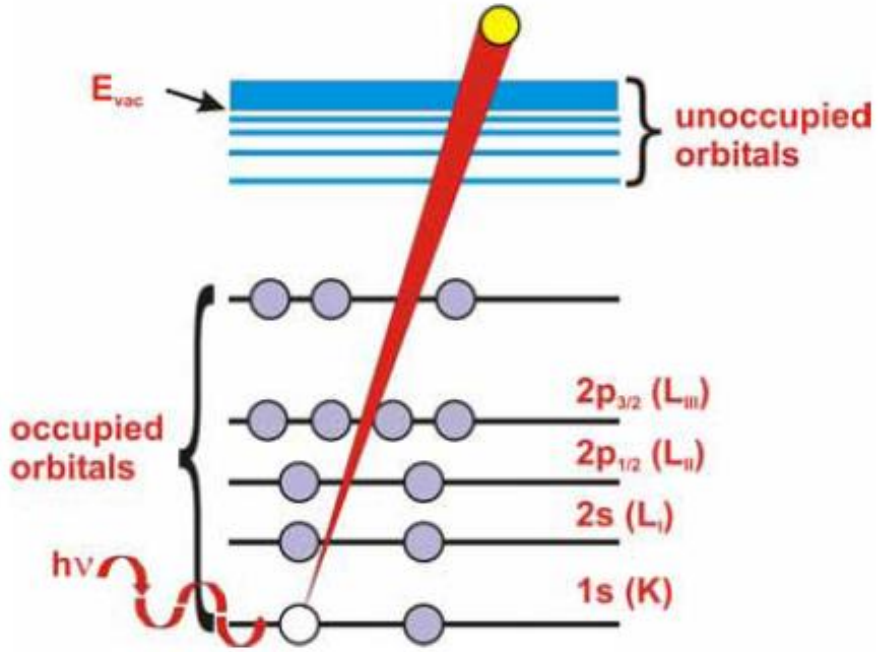

X-rays (light with wavelength 0.06- 12 Å or energy 1-200 keV) are absorbed by all matter through the photo-electric effect:

An X-ray is absorbed by an atom when the energy of the X-ray is transferred to a core level electron (K, L, or M shell) which is ejected from the atom. Any excess energy from the X-ray is given to the ejected photo-electron

FUNDAMENTALS OF XRF & XAFS TECHNIQUES: XAFS PRINCIPLE

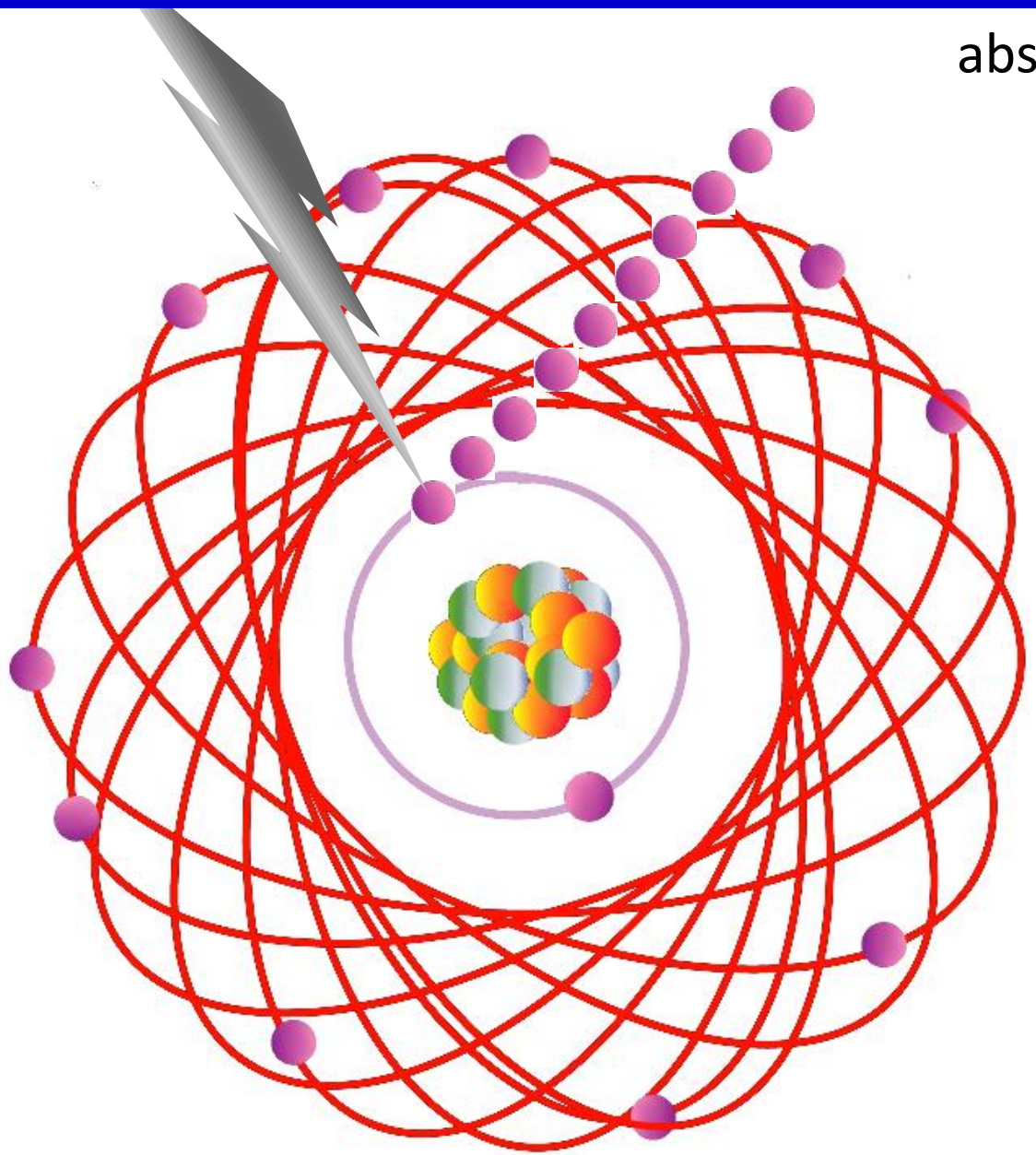

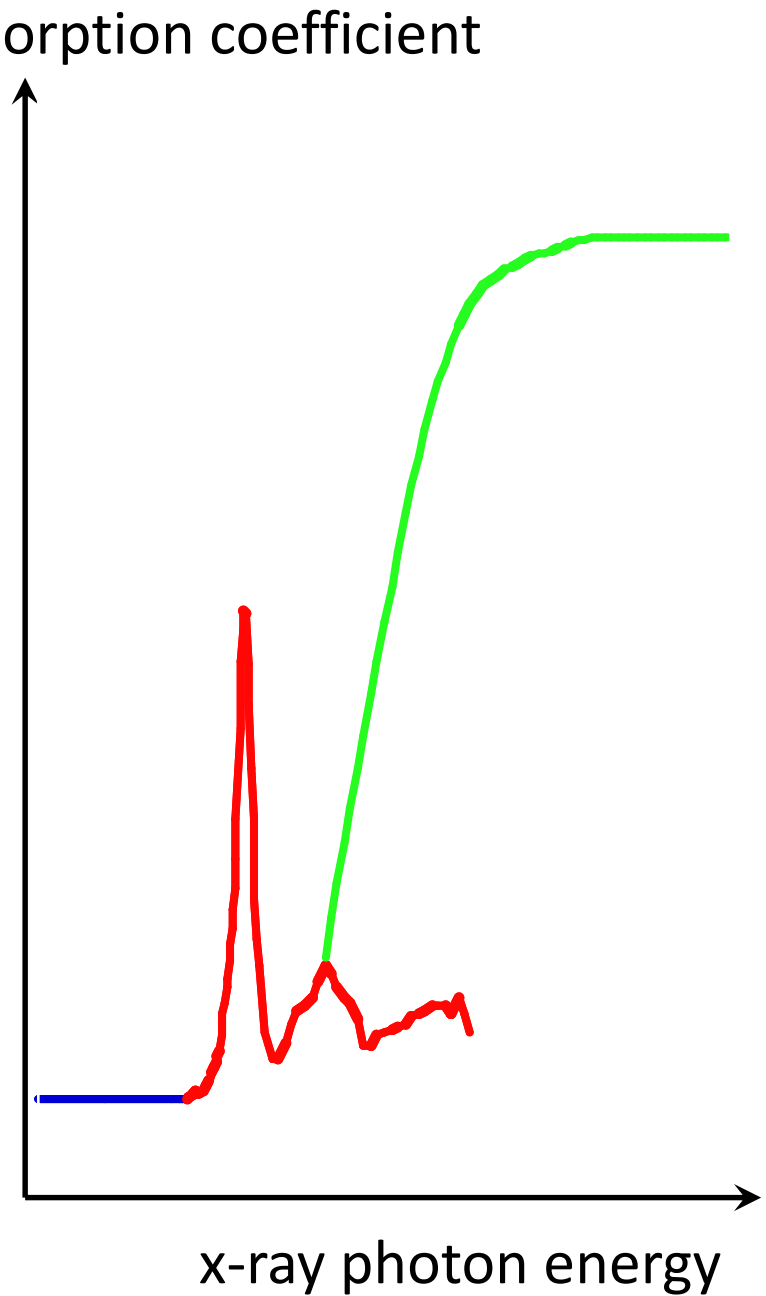

Electrons have a particle and wave nature. The photoelectron wave propagates away from the central atom (absorber), and it may scatter off neighboring atoms and finally return to its point of origin.

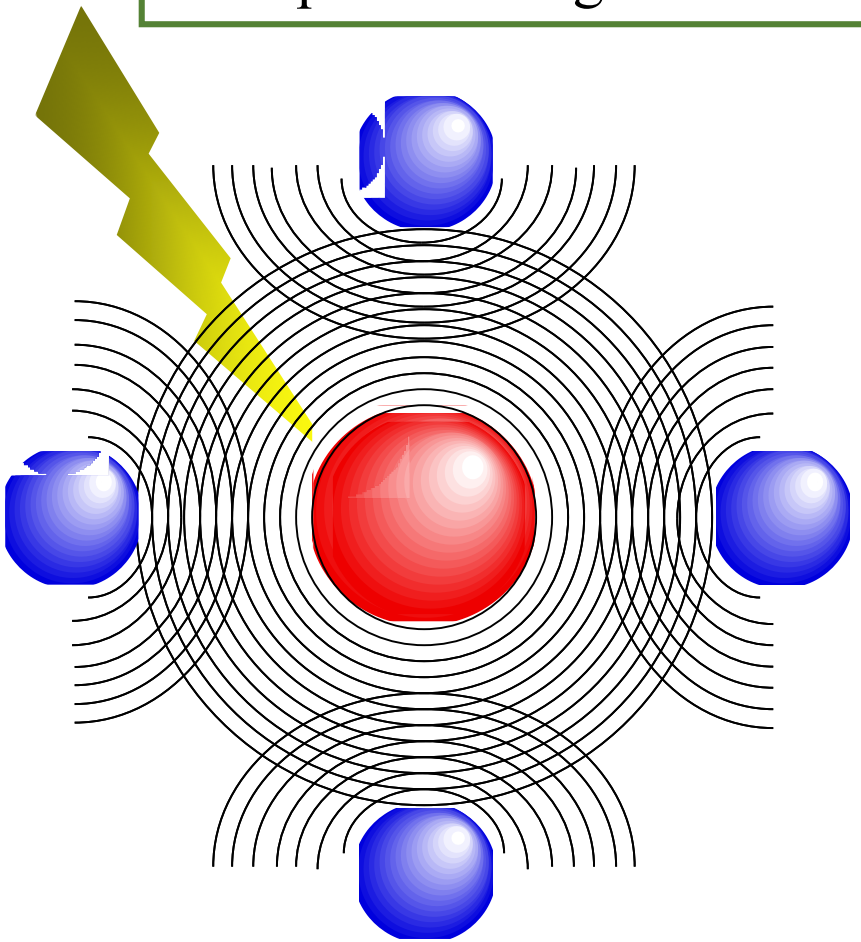

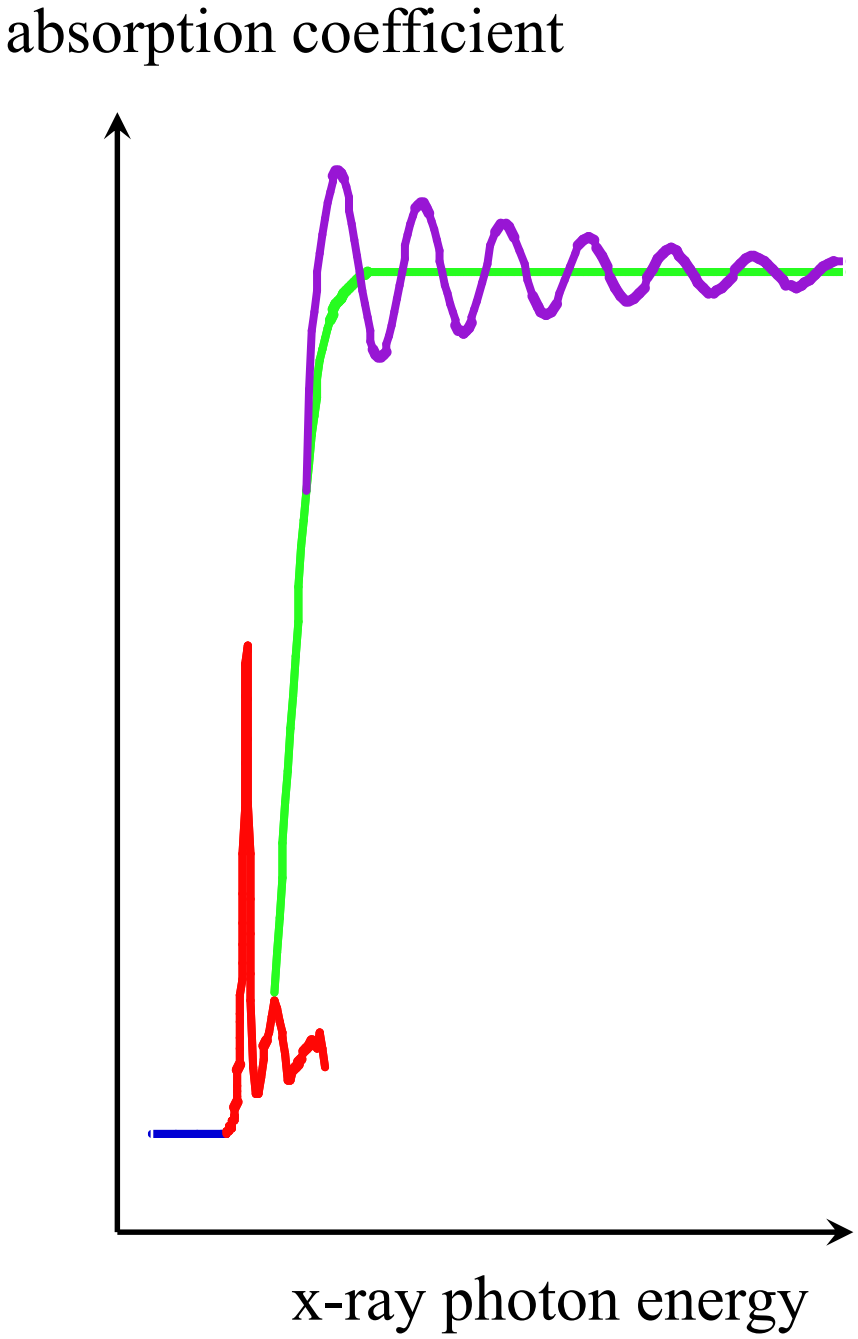

The EXAFS signal $\chi(E)$

The EXAFS signal is generally expressed as a function of the wave-vector of the photoelectron

$$k = \sqrt{\frac{2\,m\,(E - E_0)}{\hbar^2}}$$

We're interested in the energy dependent oscillations in μ(E), as these will tell us something about the neighboring atoms,

so we define the EXAFS as:

$$\chi(E) = \frac{\mu(E) - \mu_0(E)}{\Delta\mu_0(E)}$$

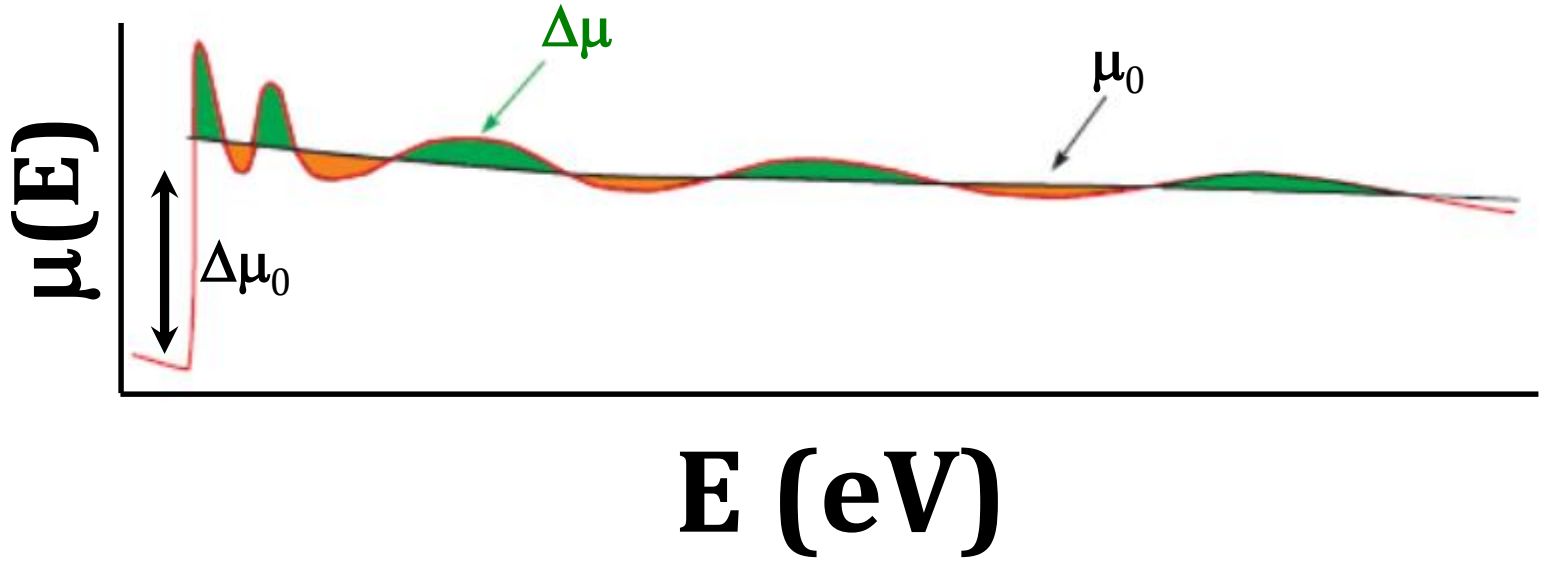

$\mu_0(E)$ Smooth function representing the bare atomic background

$\Delta\mu_0$ Edge step at the absorption edge normalized to one absorption event

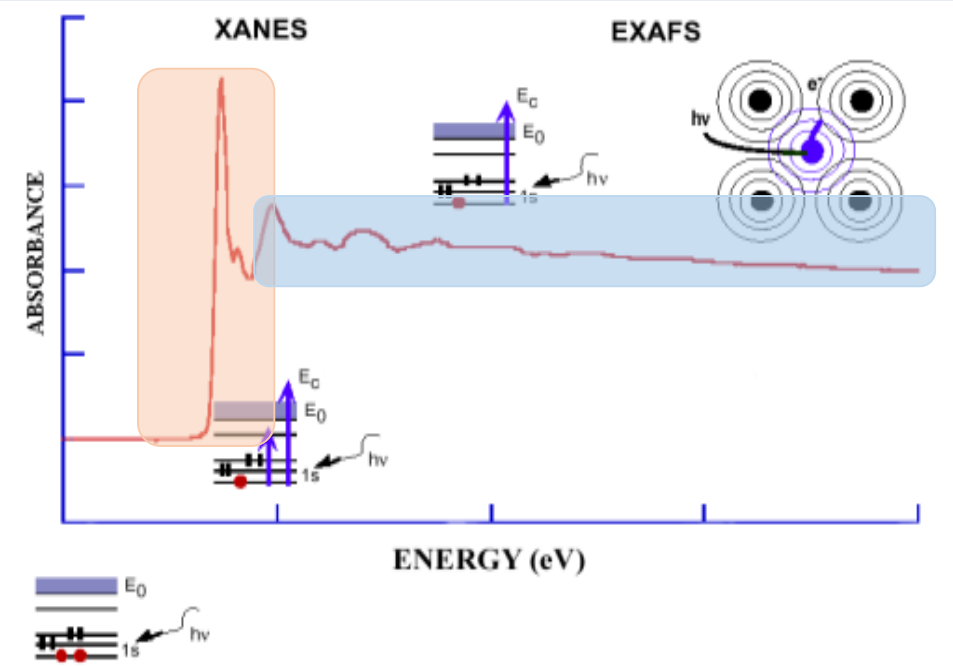

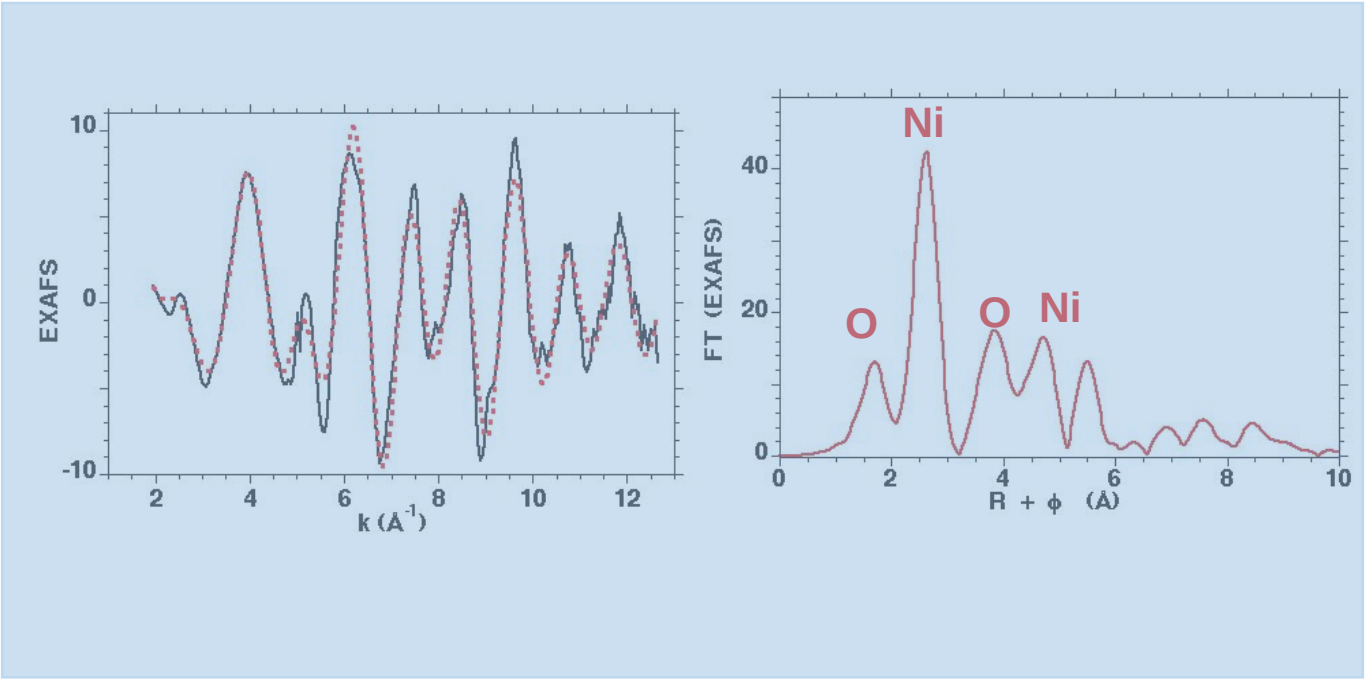

- Radial distribution of atoms around the photo-absorber (bond distance, number and type of neighbors)

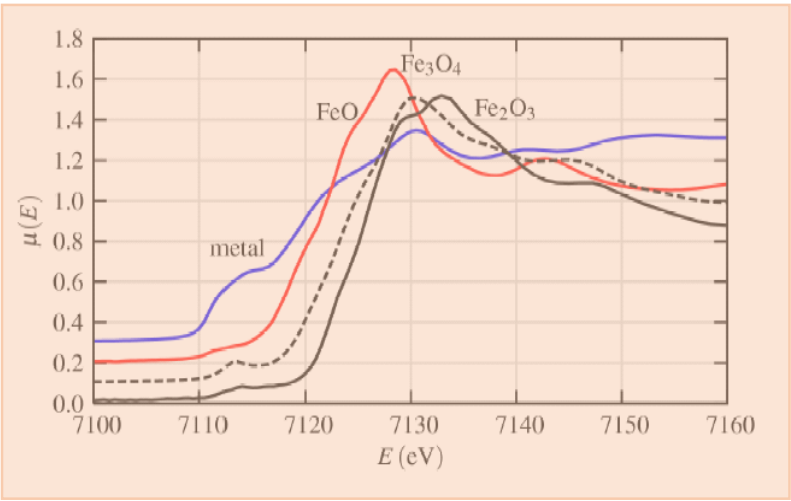

- Oxidation state
- Coordination chemistry of the absorbing atom
- Orbital occupancy

Application Domains

Environmental Science

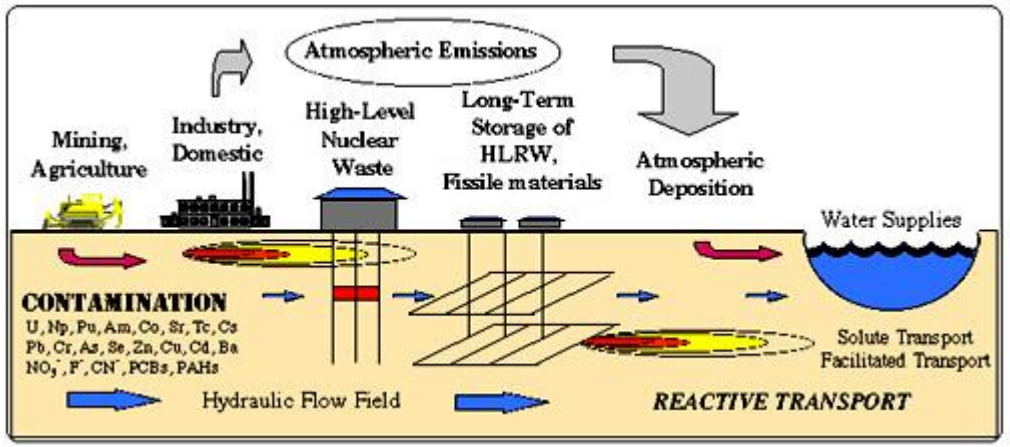

Energy *(classic & renewable)*

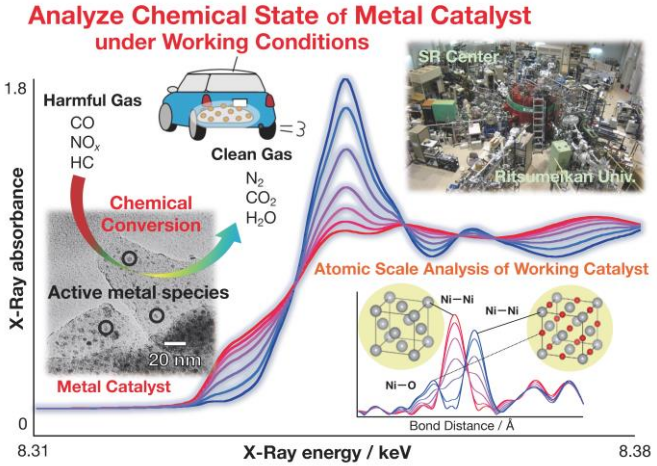

Cultural heritage and archaeology

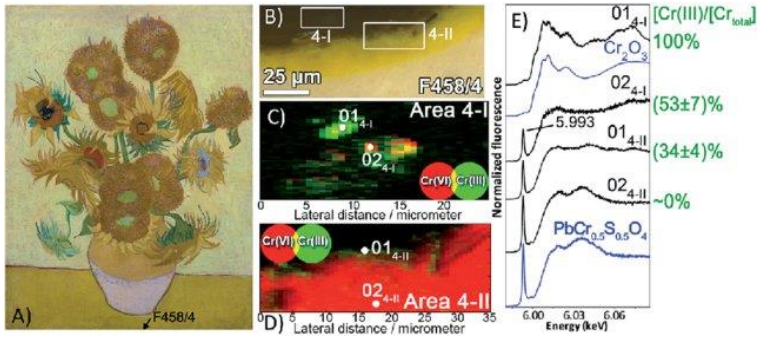

Agriculture

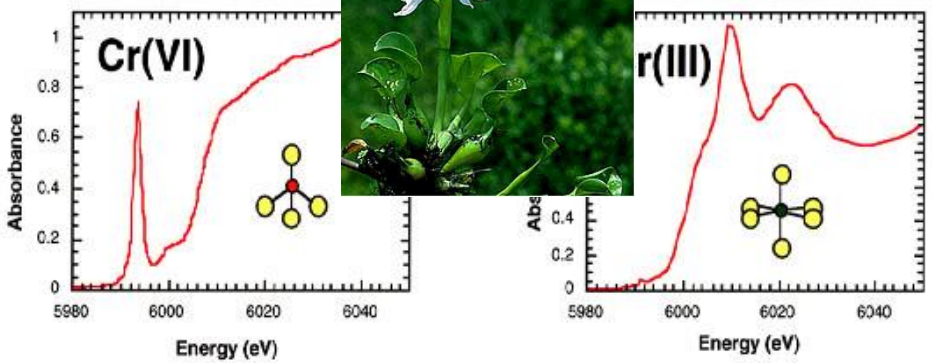

Geology & Geophysics

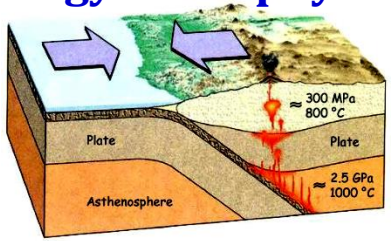

Medical and Pharmaceutical studies

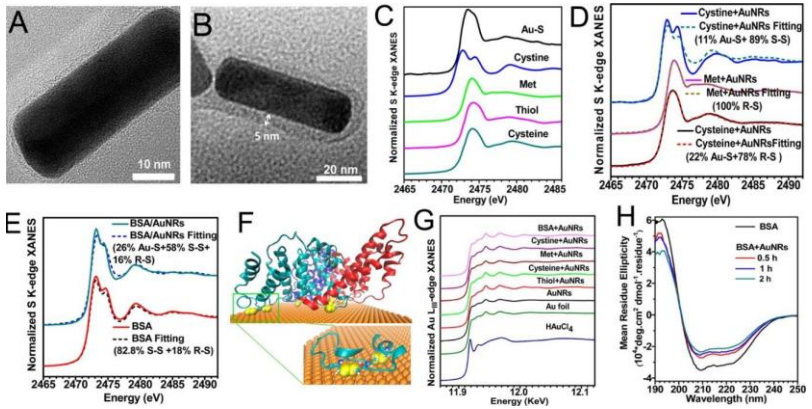

Why using XAFS

- Higher sensitivity to local distortions
- Element selectivity
- 1D radial distribution function (center at absorber)
- Charge state sensitivity (XANES)
- Investigation, with same degree of accuracy, of matter in
  - ✓ solid (crystalline or amorphous),
  - ✓ liquid solution,
  - ✓ gaseous state
- Detection of very small distortions of local structure
- Short to medium range ordering
- Need synchrotron for measurements

  ☒ Only few beamlines in each facility (XAFS/XRF @ SESAME)

RESEARCH ARTICLE DOI: 10.1002/smll.202406332

NANO · MICRO small
www.small-journal.com

İNÖNÜ ÜNİVERSİTESİ

Revealing the Role of Ruthenium on the Performance of P2-Type $Na_{0.67}Mn_{1-x}Ru_xO_2$ Cathodes for Na-Ion Full-Cells

Emine Altin, Iqra Moeez, Eunji Kwon, Ali Hussain Umar Bhatti, Seungho Yu, Kyung Yoon Chung, Muhammad Arshad, Messaoud Harfouche, Murat Buldu, Sebahat Altundag, Fatih Bulut, Sevda Sahinbay, Serdar Altin, and Mehmet Nurullah Ates**

IF: 13

Herein, P2-type layered manganese and ruthenium oxide is synthesized as an outstanding intercalation cathode material for high-energy density Na-ion batteries (NIBs). P2-type sodium deficient transition metal oxide structure, $Na_{0.67}Mn_{1-x}Ru_xO_2$ cathodes where x varied between 0.05 and 0.5 are fabricated. The partially substituted main phase where x = 0.4 exhibits the best electrochemical performance with a discharge capacity of ≈170 mAh g^{-1}. The in situ X-ray Absorption Spectroscopy (XAS) and time-resolved X-ray Diffraction (TR-XRD) measurements are performed to elucidate the neighborhood of the local structure and lattice parameters during cycling. X-ray photoelectron spectroscopy (XPS) revealed the oxygen-rich structure when Ru is introduced. Density of States (DOS) calculations revealed the Fermi-Level bandgap increases when Ru is doped, which enhances the electronic conductivity of the cathode. Furthermore, magnetization calculations revealed the presence of stronger Ru—O bonds and the stabilizing effect of Ru-doping on MnO6 octahedra. The results of Time-of-flight secondary-ion mass spectroscopy (TOF-SIMS) revealed that the Ru-doped sample has more sodium and oxygenated-based species on the surface, while the inner layers mainly contain Ru–O and Mn–O species. The full cell study demonstrated the outstanding capacity retention where the cell maintained 70% of its initial capacity at 1 C-rate after 500 cycles.

it is important to highlight the remarkable progress of Li-ion batteries (LIBs) in recent years.[1] The demand for Li-ion batteries has surged, leading to an increase in the consumption of lithium sources.[2] Newly developed electrode materials are expected to possess several key properties, including high energy density, long cycle life, and affordability for commercial feasibility.[3] It is worth noting that LIBs, first introduced by Sony in the 1990s, have become one of the most extensively used battery systems for portable electronics and various other large-scale applications.[4] Recently, there has been significant research into alternative battery types, such as lithium–sulfur (Li–S) and lithium-air (Li-air), to improve the energy density of the current state-of-the-art lithium-ion batteries (LIBs).[5] However, this progress has led to increased costs, primarily due to the limited and unevenly distributed lithium reserves around the globe.[6]

NIBs have appeared as a promising re-

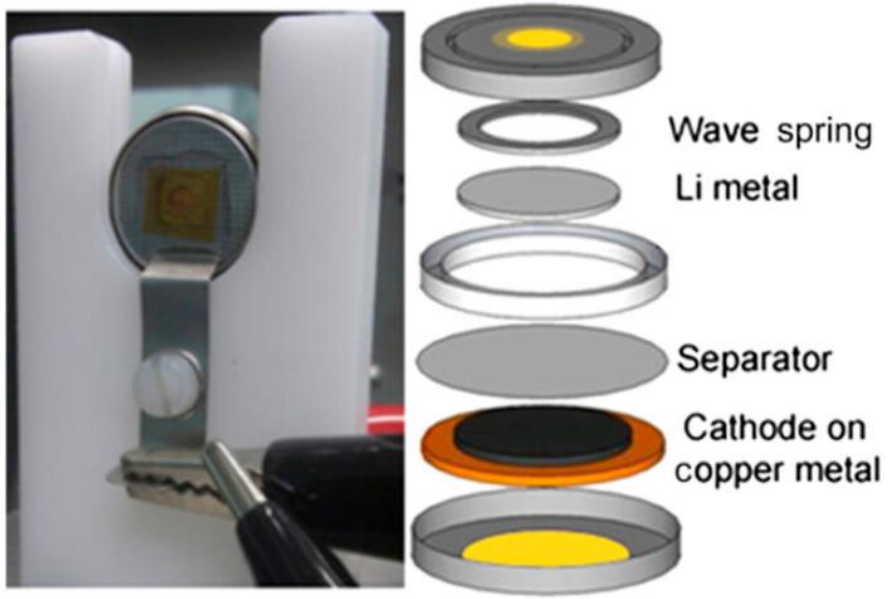

- modified version of CR2032 coin cell
- The cell allows X-ray penetration via the Kapton window.

Revealing the Role of Ruthenium on the Performance of P2-Type $Na_{0.67}Mn_{1-x}Ru_xO_2$ Cathodes for Na-Ion Full-Cells

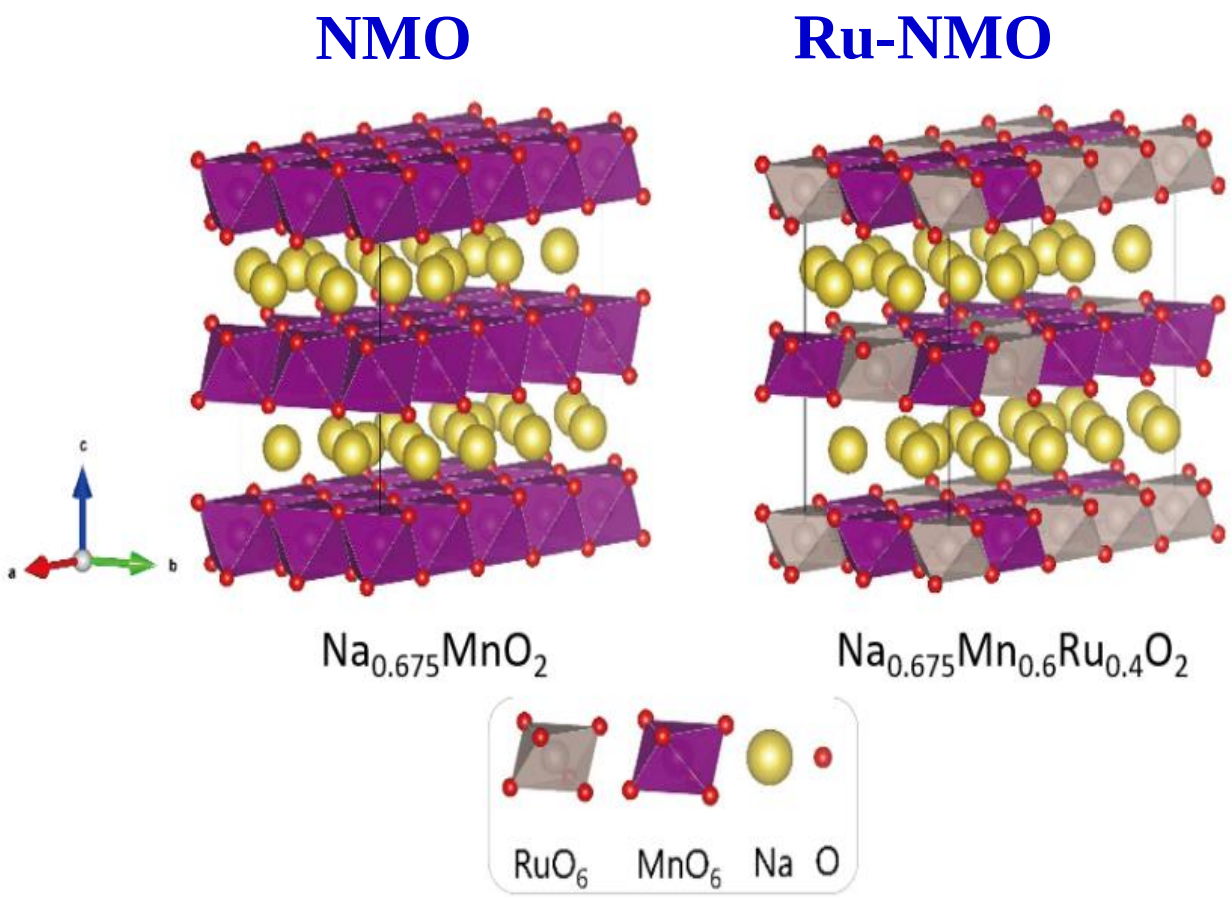

Supercell crystal structure of P2-type

Revealing the Role of Ruthenium on the Performance of P2-Type $Na_{0.67}Mn_{1-x}Ru_xO_2$ Cathodes for Na-Ion Full-Cells

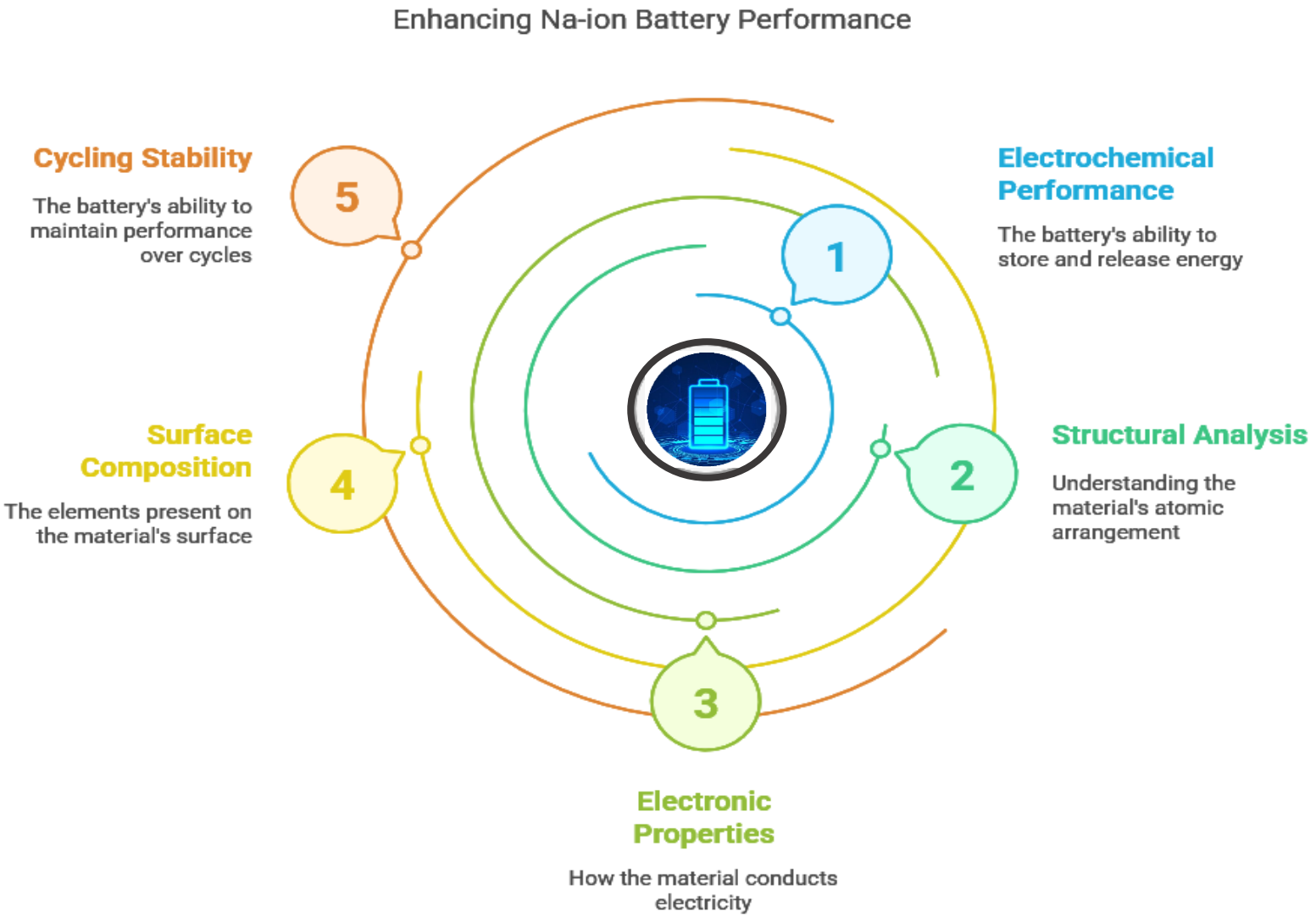

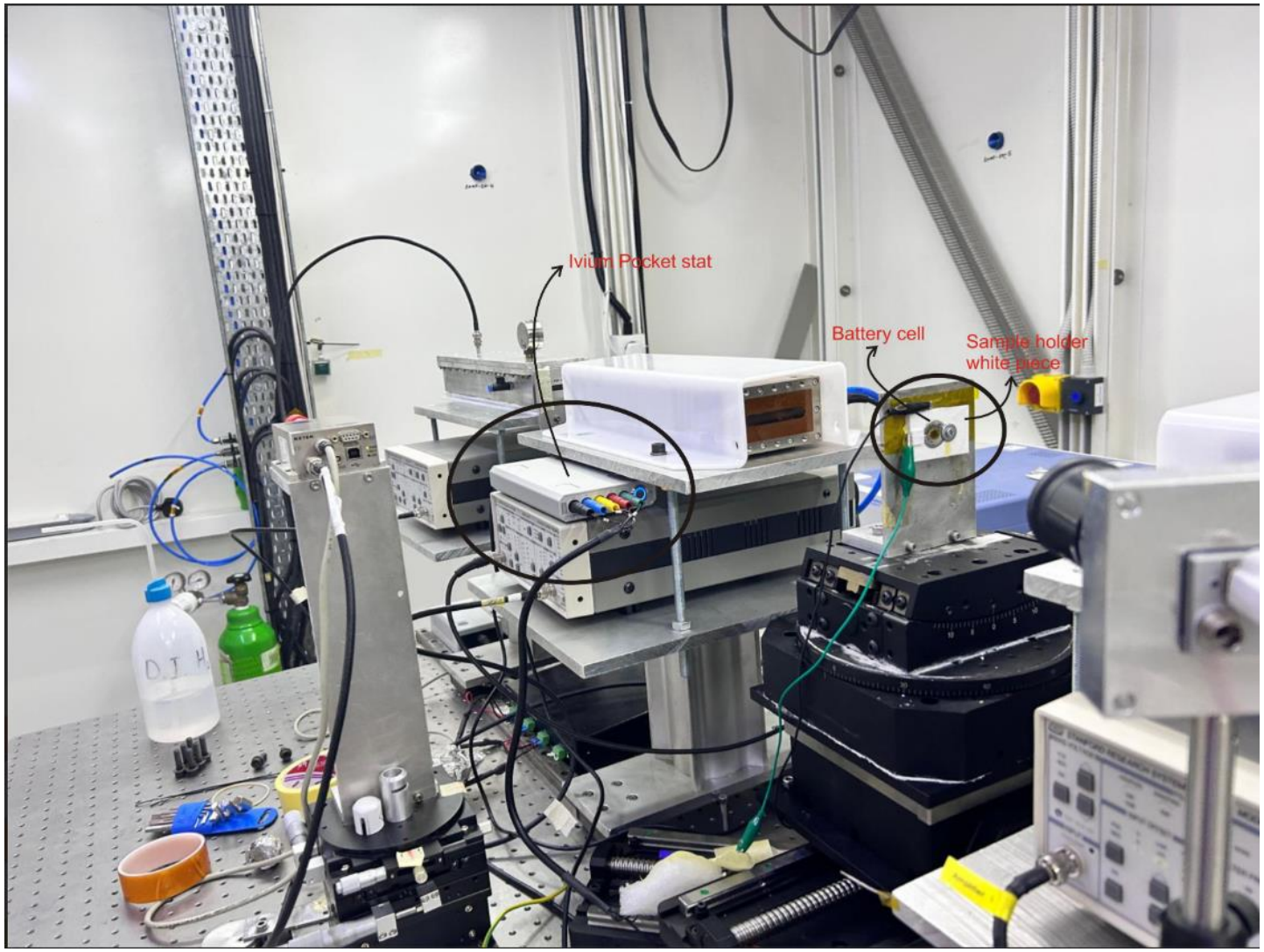
Ivium Pocket stat
Battery cell
Sample holder
white piece

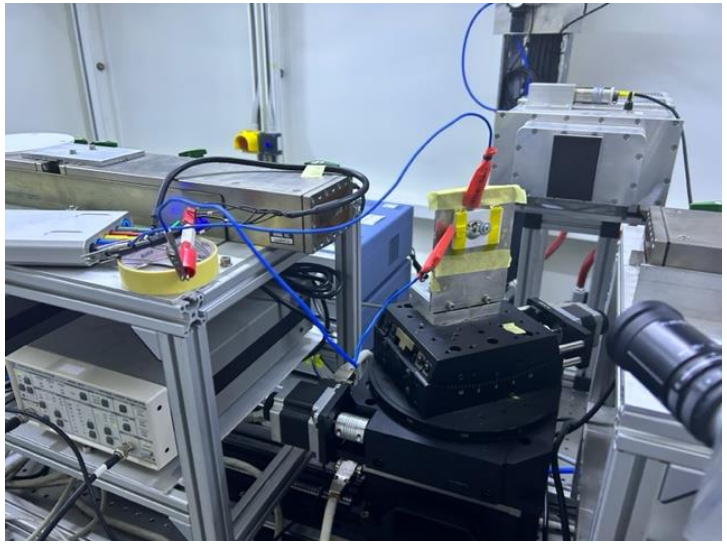

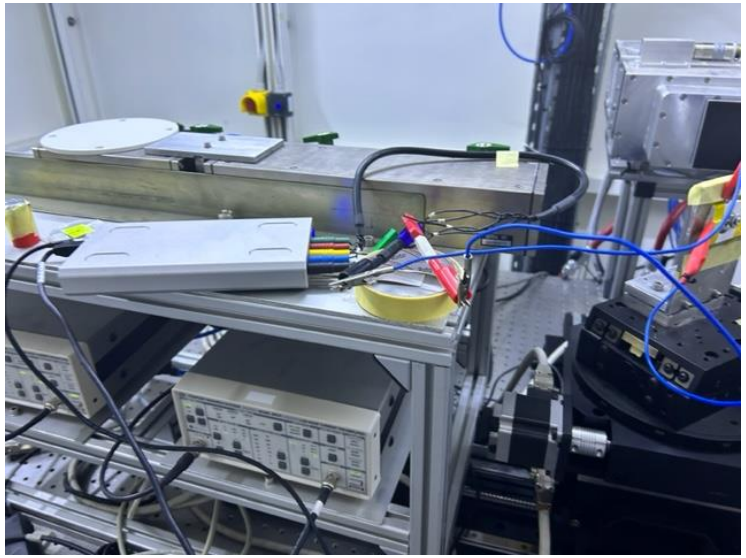

Revealing the Role of Ruthenium on the Performance of P2-Type $Na_{0.67}Mn_{1-x}Ru_xO_2$ Cathodes for Na-Ion Full-Cells

XRD Ru-substituted cathode

- It is seen that the diffraction patterns are well matched by P2-type P63/mmc symmetry, typical Na–Mn–O cathode materials
- When the Ru content increased up to x = 0.5, an impurity phase of Na_2RuO_3 is observed (C2/c symmetry)
- The other samples were free of the impurity phase, suggesting that the degree of impurity was limited to only the sample where x = 0.5

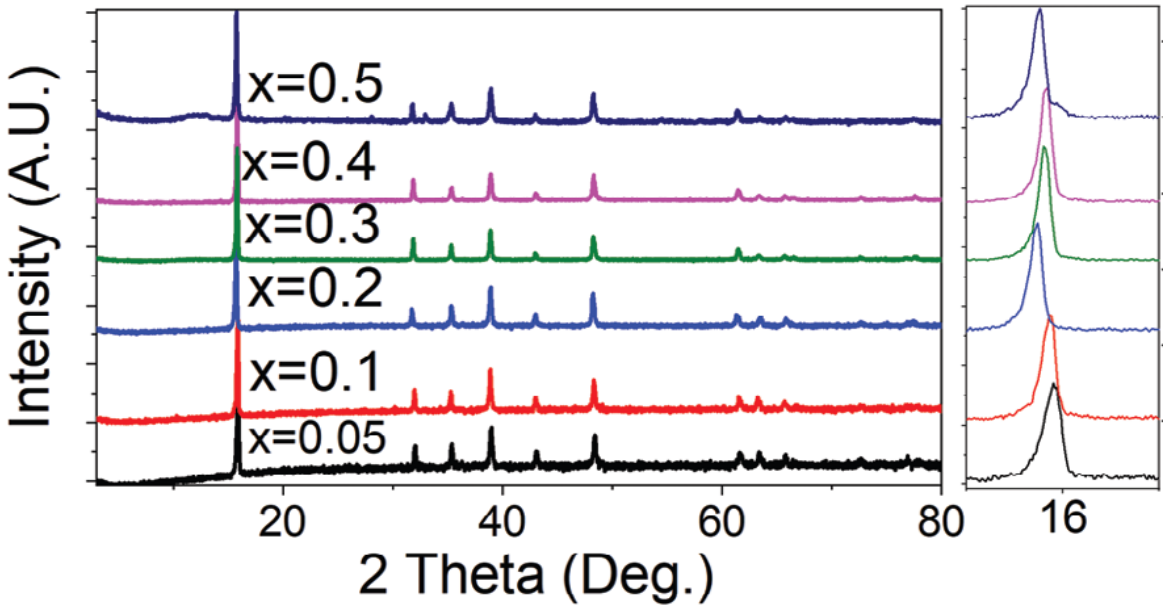

- The valence state of transition metals is influenced by the increasing amount of Ru in materials.
- The amount of Ru can affect the oxidation states of other transition metals.

Revealing the Role of Ruthenium on the Performance of P2-Type $Na_{0.67}Mn_{1-x}Ru_xO_2$ Cathodes for Na-Ion Full-Cells

Operando Structural Analysis (XRD)

- Special focus on the (002), (004), (100), and (114) peak shifts during the cycling.
- During the charging process, the solid solution mechanism is revealed by the noticeable shift of the **(004)** peak toward lower angles and the **(100)** peak toward higher angles
- An expansion along the 'c' axis and a reduction along the 'a' axis were observed.
- Lattice alterations occur during the removal of the sodium ions.

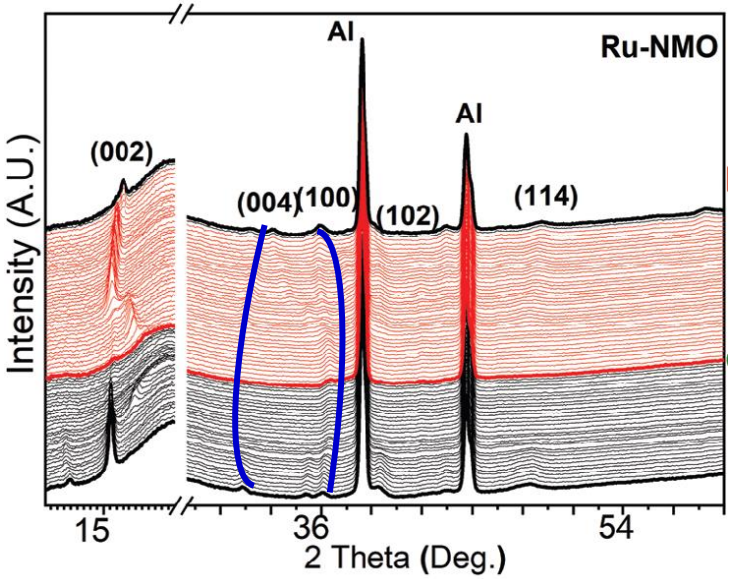

The strong peaks observed in the XRD data are due to the Al current collector.

As a result, a repulsive effect between the M-O layers takes place, instigating the expansion in the 'c' direction.

Revealing the Role of Ruthenium on the Performance of P2-Type $Na_{0.67}Mn_{1-x}Ru_xO_2$ Cathodes for Na-Ion Full-Cells

Operando Structural Analysis (XAFS)

- The XANES data was collected for the K-edge of Mn and Ru elements for the **x = 0.4 Ru** substitution cathode active material during cycling.
- Mn and Ru elements shifted toward higher energies during charging, indicating the oxidation of the Mn and Ru transition metals
- XANES peaks were observed at : 6558.8 eV and 6561.2 eV **(~2.4 eV shift**)
- Mn^{3+} ions transform to Mn^{4+} ions,
  - slightly lower oxidation state, during the charging process.

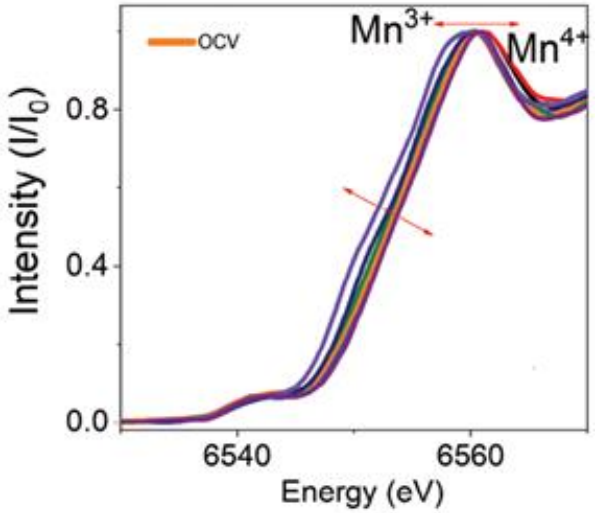

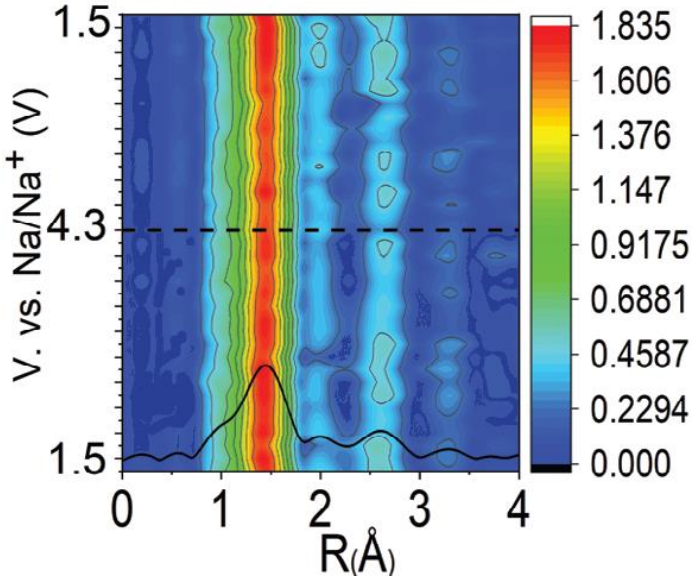

Revealing the Role of Ruthenium on the Performance of P2-Type $Na_{0.67}Mn_{1-x}Ru_xO_2$ Cathodes for Na-Ion Full-Cells

Operando Structural Analysis (XAFS)

- The XANES peaks of Ru K-edge show peaks for OCV and 4.3 V at 22,132.8 and 22,134.4 eV, (**~1.6 eV shift**).

- The XANES data for OCV corresponds to Ru^{4+}, and the spectra of Ru K-edge gradually shifted to higher energies due to the oxidation of Ru ions from 4^+ to 5^+, as indicated in the literature

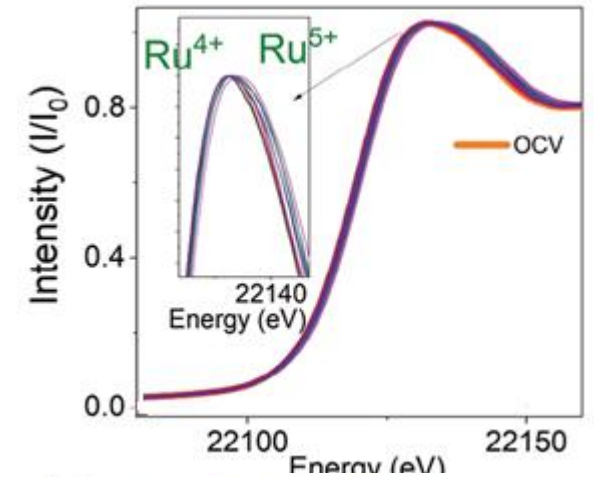

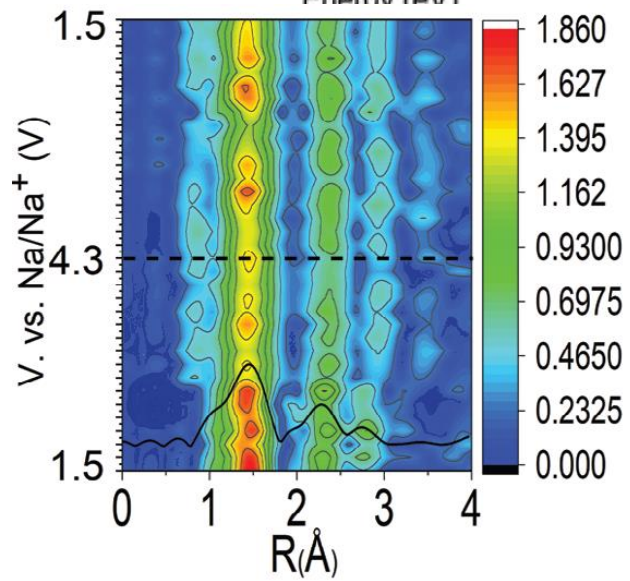

Revealing the Role of Ruthenium on the Performance of P2-Type $Na_{0.67}Mn_{1-x}Ru_xO_2$ Cathodes for Na-Ion Full-Cells

Operando Structural Analysis (XAFS)

- Mn EXAFS data fitting reveals:
  the bond lengths of Mn-O, Mn– Mn, and Mn–Ru were found to be 1.94, 2.89, and 3.20 Å.

It is expected because the repulsive force of Mn-Mn is lower than that of Mn–Ru in the structure.

- For the similar substituted elements in the form of P2-$NaMn_{0.9}Fe_{0.1}O_2$, bond lengths were increased 1.998 Å (Mn–O) and 2.905Å (Mn–TM) by Ru doping.

x=0.4 Ru substituted cells

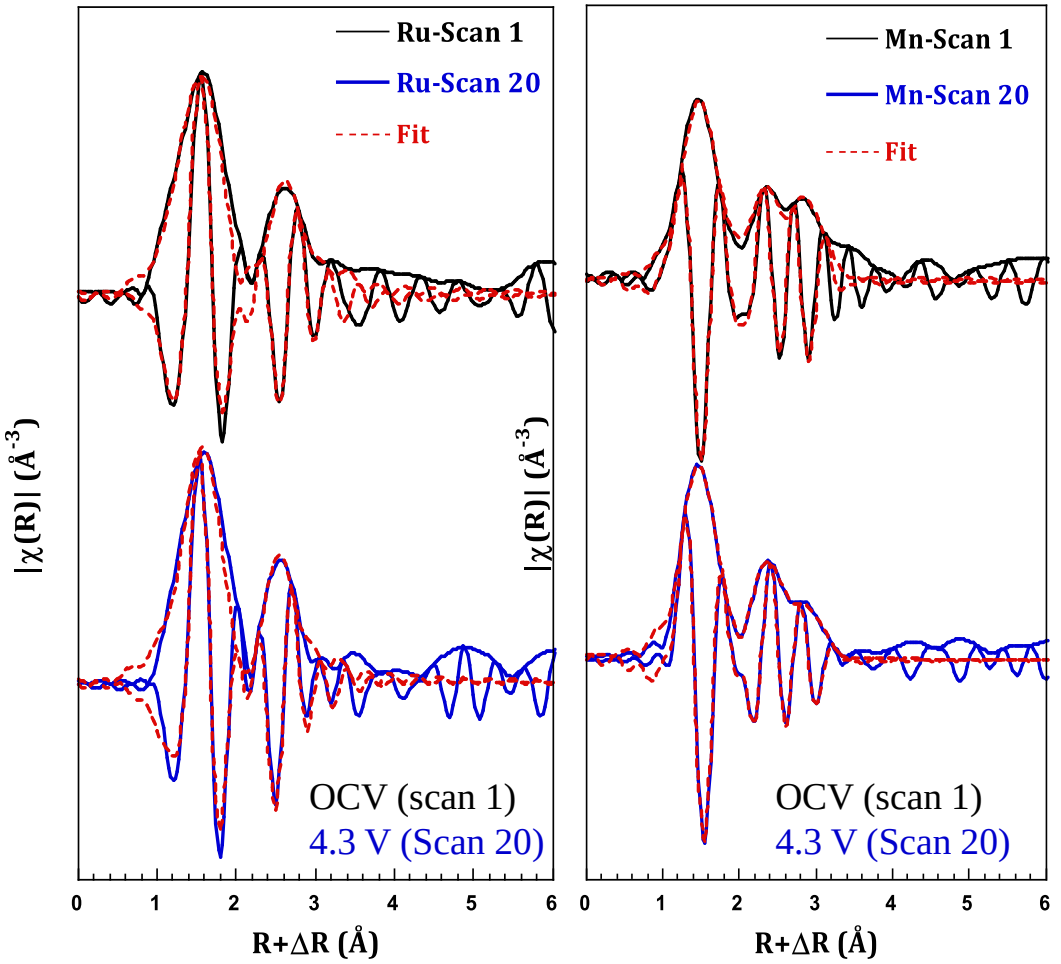

In contrast, the Ru-O bond length was not affected during charging/discharging process, providing a more stable structure.

Similar work but for $Na_{0.67}Mn_{1-x}Fe_xO_2$

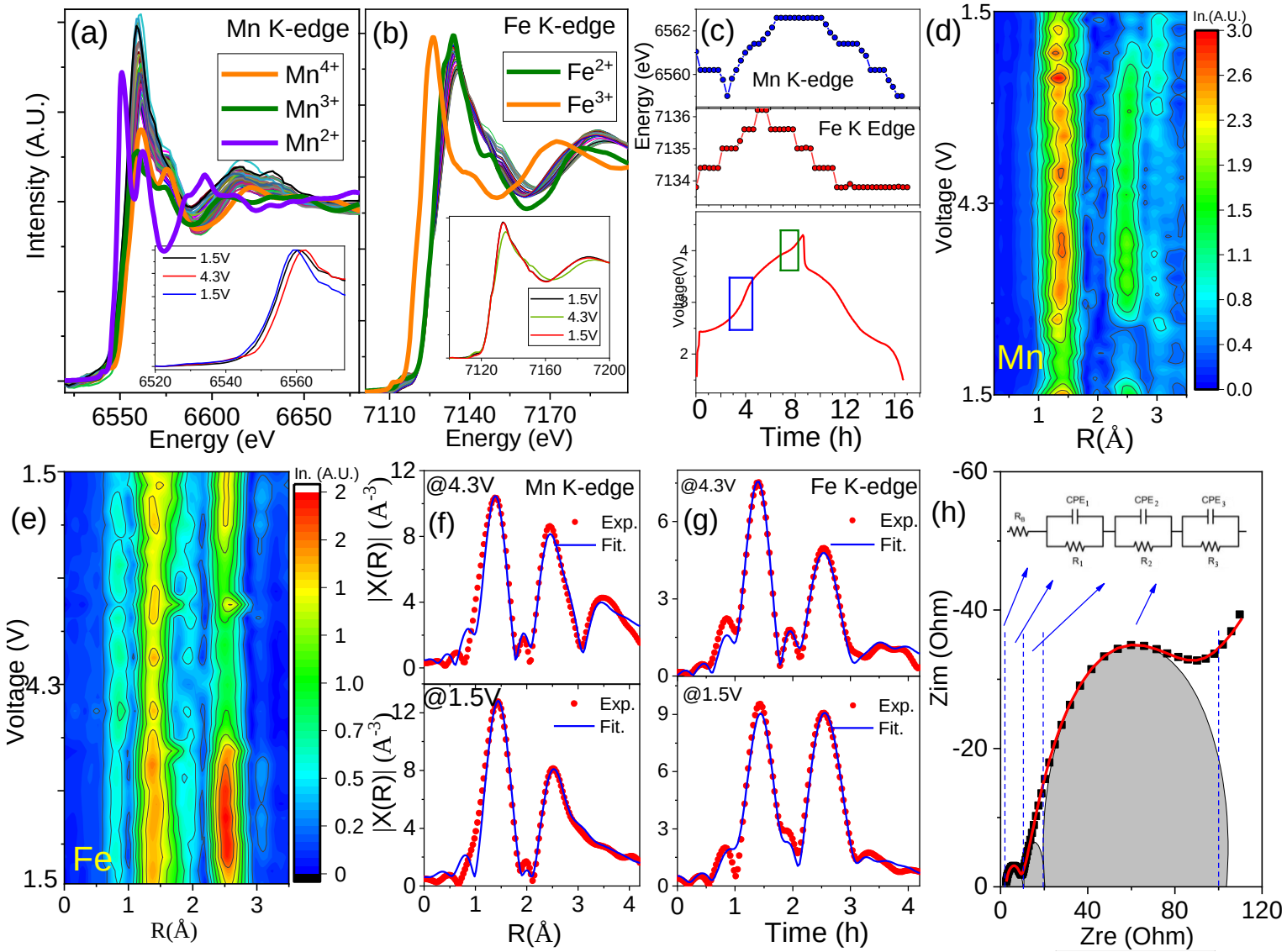

- In-situ XANES spectrum of (a) Mn and (b) Fe k-edge of the x=0.5 cathode, (c) peak values graphs depending on the voltage, in-situ XAFS mapping graphs of (d) Mn-k-edge and (e) Fe K-edges, artemis model analysis of (f) for Mn and (g) Fe K-edges and (h) EIS analysis of full cells of x=0.5 carbon battery

Bilkent University

Tungsten Oxide Disproportionation Under Constant Voltage: XAFS study

Burak ULGUT

Bilkent University - Dept. of Chemistry (TURKEYE)

Acknowledgment:

Argonne NATIONAL LABORATORY
Si (311) crystals

HZDR
HELMHOLTZ ZENTRUM DRESDEN ROSSENDORF
ROBL beamline, Germany (Optics)

SOLEIL SYNCHROTRON

SESAME
All SESAME Staff
- Scientific
- Technical
- Administration

IAEA International Atomic Energy Agency
-XEOL
-Components
-Equipments

INFN Istituto Nazionale di Fisica Nucleare
Elettra Sincrotrone Trieste
64- El SDDetector

LNLS sirius Laboratório Nacional de Luz Síncrotron

İNÖNÜ ÜNİVERSİTESİ

Bilkent University

diamond
DCM

SESAME

Synchrotron-light for Experimental Science and Applications in the Middle East

Thank you For Your Attention

https://www.sesame.org.jo/beamlines/xafs-xrf

Messaoud.Harfouche@sesame.org.jo
Latifullah.Khan@sesame.org.jo